IEEE Access
Multidisciplinary | Rapid Review | Open Access Journal

Received 5 July 2024, accepted 14 July 2024, date of publication 29 July 2024, date of current version 6 August 2024.

Digital Object Identifier 10.1109/ACCESS.2024.3434675

RESEARCH ARTICLE

Exploring CEEMDAN and LMD Domains Entropy Features for Decoding EEG-Based Emotion Patterns

NALINI PUSARLA[1,2], ANURAG SINGH[1], (Member, IEEE), SHRIVISHAL TRIPATHI[1], (Senior Member, IEEE), AVINASH VUJJI[3], AND RAM BILAS PACHORI[4], (Senior Member, IEEE)

[1]Department of Electronics and Communication Engineering, International Institute of Information Technology, Naya Raipur, Naya Raipur, Chhattisgarh 493661, India
[2]Department of Electronics and Communication Engineering, Vignan's Institute of Information Technology, Visakhapatnam, Andhra Pradesh 530049, India
[3]Department of Electrical and Electronics Engineering, Vignan's Institute of Engineering for Women, Visakhapatnam, Andhra Pradesh 530046, India
[4]Department of Electrical Engineering, Indian Institute of Technology Indore, Indore 452017, India

Corresponding author: Nalini Pusarla (nalini@iiitnr.edu.in)

ABSTRACT Electroencephalogram (EEG) signal-based emotion classification is vital in the ever-growing human-computer interface (HCI) applications. However, the chaotic, non-stationary, and person-dependent nature of EEG signals often limits such practical applications. These challenges reduce the ability of the state-of-the-art approaches to effectively distinguish between different emotional states from EEG data, resulting in sub-optimal emotion recognition performance. This work presented a time-frequency (T-F) analysis of EEG signals to localize different EEG frequency rhythms responsible for emotion-related information in the EEG signals. In particular, this work investigated two T-F analysis domains for multichannel EEG signals based on complete ensemble empirical mode decomposition with adaptive noise (CEEMDAN) and local mean decomposition (LMD) to extract entropy features that capture specific emotion-relevant traits from the specific EEG channels that are highly responsive to emotions. The CEEMDAN and LMD decompose the EEG signals into different EEG frequency rhythms called mode functions, intrinsic mode functions (IMFs), and product functions (PFs), respectively. Further, various types of entropy feature of these two categories of mode functions, such as approximate entropy (ApEn), sample entropy (SaEn), permutation entropy (PeEn), and bubble entropy (BuEn), are computed for extracting emotion-relevant distinguishing features. Entropy features help quantify EEG's non-linear behavior and eventually help classify EEG-based emotions precisely. Emotion classification has been achieved using a grid search cross-validation (GSCV) optimized XGboost classifier. Thorough experimentations are conducted to validate the efficacy of the proposed approach on publically accessible datasets named Database for Emotion Analysis of Physiological Signals (DEAP), SJTU emotion EEG dataset (SEED), and SEED-IV. The efficacy of the proposed emotion recognition approach is measured in terms of widely used performance metrics such as accuracy, confusion metrics, receiver operating characteristics (RoC), and area under the curve (AuC). The highest average accuracy is attained using the proposed LMD-domain BuEn features, i.e., 97.8%, 98.6%, and 95.7% using SEED, SEED-IV, and DEAP databases, respectively, outperforming the recent state-of-the-art emotion recognition algorithms.

INDEX TERMS CEEMDAN, LMD, XGboost, bubble entropy, grid search, cross-validation and emotion recognition.

I. INTRODUCTION

Emotions are fundamental human traits that significantly influence our daily activities, including cognition,

The associate editor coordinating the review of this manuscript and approving it for publication was M. Sabarimalai Manikandan.

© 2024 The Authors. This work is licensed under a Creative Commons Attribution-NonCommercial-NoDerivatives 4.0 License.
For more information, see https://creativecommons.org/licenses/by-nc-nd/4.0/

decision-making, and intelligence. Beyond logical reasoning, emotional capability is crucial to human intellect [1]. The advancement of emotional artificial intelligence is a prominent trend in human-computer interaction (HCI) research [2]. In addition to their role in emotional intelligence, emotions are directly linked to various mental illnesses such as depression, attention deficit hyperactivity disorder (ADHD), autism, and gaming addiction [3]. Consequently, emotional computing has emerged as a multidisciplinary research field aimed at developing human-aware artificial intelligence capable of recognizing, understanding, and regulating emotions [4]. Affective computing primarily detects and simulates human emotions using pattern analysis and machine learning techniques. Among the various methods, emotion recognition through EEG data has proven more reliable than frameworks that rely on outward appearances, such as facial expressions, gestures, and speech signals, which can be manipulated to display fake emotions [5]. Although EEG has limited spatial resolution, it offers high temporal resolution, allowing for evaluating signal properties associated with emotional inputs. Additionally, EEG is a cost-effective, quick, and non-invasive technique, making it a prominent choice for studying brain reactions to emotional stimuli [6]. EEG has become a crucial technology for HCI systems, enabling the quantification of neurological activity from the brain via contact electrodes attached to the scalp. Moreover, the temporal resolution of EEG, which is significantly faster than the pace of emotional changes, offers a substantial advantage in accurately capturing and analyzing emotional responses [7]. As a result, EEG can collect, track, and distinguish dynamic changes in brain activity. However, EEG-based emotion recognition remains highly challenging due to the indistinct boundaries between various emotions. Additionally, EEG signals are highly asymmetrical and non-stationary, leading to variations in EEG rhythms and emotional signatures among individuals, even for the same emotion. This phenomenon, subject-independent or cross-subject emotion recognition, further complicates EEG's emotion detection process. In numerous studies on EEG-based emotion recognition, multichannel EEG recordings, capturing signals from various brain regions, are employed. However, not all channels contribute equally to reflecting the subject's emotions. As a result, examining data from all channels can lead to redundancy and duplication [13]. Few studies have addressed the specific EEG channel selection responsible for detecting emotions. In [14], four distinct channel profiles were utilized, demonstrating superior performance in emotion detection compared to all channels. More recently, researchers in [15] selected 14 emotion-significant channels from the DEAP dataset, achieving improved emotion classification performance. Recently, 25 channels from the SEED dataset were employed for emotion detection, achieving a reported accuracy of 89.32% by combining particle swarm optimization for feature reduction with a fusion of convolutional neural network (CNN) and long short-term memory (LSTM) architectures [44]. In the literature, numerous methods have been reported for analyzing human emotions via EEG, utilizing various feature extraction procedures. Time-frequency (T-F) domain-based techniques have rapidly gained popularity due to their ability to extract distinctive EEG features. These techniques include independent component analysis (ICA), short-time Fourier transforms (STFT) [16], empirical mode decomposition (EMD) [17], [18], wavelet transform (WT) [19], and others. However, these approaches have certain limitations. Few studies [17], [18] have utilized EMD to divide EEG signals into intrinsic mode functions (IMFs), from which various attributes were derived. However, EMD has limitations such as mode mixing, noisy modes, and deviating intermediate frequencies [20]. Advanced approaches like ensemble empirical mode decomposition (EEMD) and complete ensemble EMD with adaptive noise (CEEMDAN) have been developed to address the limitations of conventional EMD, such as mode mixing [21]. However, these methods are computationally intensive and are limited in real-world applications [20], [47]. In contrast, local mean decomposition (LMD) offers a more efficient and accurate analysis of EEG signals. LMD generates product functions (PFs) that better represent the input signal than the IMFs produced by EMD methods. Additionally, LMD calculates instantaneous frequency (IF) in one pass, avoiding the boundary effects and inaccuracies associated with the Hilbert transform used in EMD. Thus, LMD is more effective for tasks such as emotion detection in EEG signals, providing deeper insights and reducing computational complexity [20].Thus, the LMD-decomposed EEG signal aids in capturing non-linear EEG aspects that are vital for emotion interpretation. This work presented a comparative analysis of CEEMDAN and LMD for T-F analysis of EEG signals for emotion recognition application. Consequently, the T-F analysis of EEG signals has resulted in mode functions, further analyzed using non-linear techniques to capture non-linear characteristics such as fractal dimension (FD) [62] and entropy metrics. Conventional FD metrics focus solely on the complexity of a time series at one specific time scale, failing to capture its comprehensive complexity [62]. Consequently, two variants of FD are proposed to overcome the limitations of conventional FD metrics [62]. However, entropy-based techniques like approximate entropy (ApEn) [24], sample entropy (SaEn) [24], [25], permutation entropy (PeEn) [27], dispersion entropy [63], and slope entropy [64] are mostly employed for evaluating the complexity of time series data. Out of these, ApEn, SaEn, and PeEn have been frequently used for different EEG-based applications [21], [22], [23], [24], [25], [26]. However, there are certain limitations to these existing entropy measures. Generally, entropy techniques depend highly on the parameters, i.e., threshold/tolerance and the subsequence length [25]. Due to this, the performance of the entropy measures in the form of discriminating power, tolerance to artifacts, or any other essential feature can vary

significantly depending on the values of these parameters. Consequently, selecting internal parameters is a crucial fact of entropy computations. This challenge motivated us to explore bubble entropy (BuEn) features within the LMD domain, which have not yet been investigated for emotion recognition tasks. Since BuEn is practically free of internal parameters [27], it helps achieve stable emotional discriminating ability from EEG signals. Moreover, LMD-decomposed PFs are noise-free and help capture different EEG rhythms. Thus, this work computed the BuEn of CEEMDAN-IMFs and LMD-PFs to get more specific details or events of emotion from EEG signals and presented a comparative analysis of emotion classification. This study also showed a comparative analysis with the existing entropy techniques. It demonstrated that the BuEn features computed on LMD domain PFs outperform the current entropy features captured through ApEn, SaEn, and PeEn for emotion classification.

Recent advances in emotion identification studies involve cutting-edge machine learning and deep learning algorithms that use manual EEG features and automated or image-like attributes. Deep learning techniques reported recently with good EEG-based emotion recognition performance include CNN-LSTM [15], [40], a fusion of CNN and recurrent neural network (RNN), i.e., ACRNN [28], a fusion of CNN, stacked autoencoder (SAE) and dense neural network (DNN) [29], asymmetric CNN [30], deep CNN [31] with feature dimension reduction strategy. Despite achieving high accuracy, the work in [28] is computationally complex as it combines three deep models (i.e., CNN, SAE, and DNN) for feature extraction, feature reduction, and classification. Additionally, it used advanced techniques, including extracting Pearson correlation coefficient characteristics for emotion categorization and transforming EEG into 2D images. A few complex hybrid deep networks, like in [41], have recently been employed for emotion recognition with a manual feature extraction approach. However, only marginal improvements could be achieved using the DEAP dataset compared to the state-of-the-art methods [42], [43], [45], [46]. However, higher accuracy is obtained with SEED and SEED-IV datasets. Out of these [42], achieved high accuracy but involved many stages to perform the recognition task, such as the Relief algorithm for channel selection, max-relevance, and min-redundancy algorithm to obtain emotion-relevant channels further and combined EEGNet [50] with capsule network resulting in EEGNet for emotion- recognition. Moreover, [45] also used a hybrid model, i.e., attention-based convolutional transformer neural network (ACTNN) that cascades CNN and transformer fed with two features, i.e., a spatial feature made into a 2D matrix and spectral characteristics of EEG frequency rhythms. It is worth mentioning that hybrid-deep techniques are resource-intensive and data-hungry. These observations motivated us to propose an emotion recognition framework using T-F domain nonlinear features and an ML-based classifier.

The contributions of the proposed work are summarized as follows:

- A new method for emotion recognition is proposed based on time-frequency (T-F) analysis of EEG signals, utilizing CEEMDAN and LMD techniques. This approach effectively captures different EEG frequency rhythms associated with various emotion patterns.
- To capture the non-linear behavior of the T-F decomposed EEG, entropy-based features of the mode functions are proposed, which aids in further localizing the emotion-aware traits of the EEG.
- An XGboost model optimized via grid search cross-validation (GSCV) is developed, improving the classifier's ability to accurately identify emotions by fine-tuning its hyperparameters.
- An analysis based on EEG channel profiles is conducted to determine the most effective channel configurations for capturing emotion-relevant information, thus enhancing the emotion recognition task.
- Cross-subject validation (CSV) and cross-dataset validation (CDV) are carried out to assess the robustness of the proposed approach in handling inter-subject variability, ensuring the model's reliability and generalizability across different subjects and datasets.

II. DATASET DETAILS

The public domain databases SEED [14], SEED-IV [48], and DEAP [49] have been used to assess the effectiveness of the proposed work. The details of the databases are discussed in the following sections and summarized in Table 1.

A. SEED DATASET

The SEED dataset focuses on EEG signals from 15 subjects who watched 15 four-minute film clips to elicit positive, neutral, and negative emotions. The EEG data is recorded using 62 channels, providing high-resolution information on brain activity. Data collection across three sessions ensures consistency and allows analyzing emotion recognition reliability over time. This session-based structure is precious for understanding how emotional responses can vary or remain stable across different times, enhancing the robustness of emotion recognition models. SEED's detailed EEG recordings enable in-depth analysis of the brain's emotional responses, making it a vital resource for researchers aiming to develop precise and reliable emotion recognition systems.

B. SEED-IV DATASET

SEED-IV builds on the SEED dataset by expanding the range of emotional stimuli and classes. It includes EEG data from 15 subjects who watched 72 two-minute film clips to elicit happy, sad, fearful, and neutral emotions. Like SEED, the EEG data is captured using 62 channels and collected across multiple sessions. This expanded dataset provides a broader spectrum of emotional data, crucial for training models distinguishing between various emotional states. The numerous sessions help study the temporal stability of emotional responses, ensuring that the models developed are accurate and consistent over time. SEED-IV's comprehensive

TABLE 1. Database information.

Database	Array Title	Array information
SEED	EEG samples	15clips x 62channels x 48000 datapoints
	Labels	Three emotion classes
SEED-IV	EEG samples	24clips x 62 channels x 48000 datapoints
	Labels	Four emotion classes
DEAP	EEG samples	40clips x 40 channels x 8064 datapoints
	Labels	Four emotion classes

and varied emotional stimuli make it an invaluable dataset for advancing the capabilities of EEG-based emotion recognition systems, allowing for more nuanced and accurate detection of emotional states [48].

C. DEAP DATASET

The DEAP dataset is a comprehensive resource for EEG-based emotion recognition, comprising data from 32 participants who watched 40 one-minute music videos intended to evoke various emotional responses. The dataset includes 32-channel EEG recordings, providing a detailed view of brain activity during these emotional experiences. Participants also offered self-assessed ratings for arousal, valence, like/dislike, dominance, and familiarity, which are crucial for mapping EEG patterns to specific emotional states. The large number of participants and stimuli ensures a diverse dataset, capturing a wide range of emotional responses, essential for developing robust and generalized emotion recognition models. DEAP's extensive annotations and high-quality EEG data make it a benchmark in the field, facilitating the creation of reliable and accurate systems for detecting and interpreting emotions based on brain activity.

III. PREPROCESSING

Different types of noise also get captured during EEG data acquisition. So, EEG data records need to be preprocessed regarding noise removal, filtering, downsampling, etc., so that the resultant data is ready for subsequent analysis. The EEG data records taken from the publicly available databases, DEAP, SEED, and SEED-IV, have already been preprocessed to some extent. For example, in the DEAP dataset, the acquired EEG was initially down-sampled, bringing the sampling frequency down to 128 Hz. Next, a band-pass filter was applied, restricting the signal to the 4–45 Hz range. Each trial lasted 63 seconds, with the first 3 seconds serving as preparation time and the subsequent 60 seconds dedicated to video observation. Consequently, each trial consists of 8,064 sampling points for each channel [49]. In the case of the SEED and SEED-IV datasets, the preprocessing steps include downsampling the EEG data to 200 Hz, a band pass filtering with a throughput frequency range of 1-75 Hz, and extracting EEG trails corresponding to the duration of each video. These preprocessing steps are essential for refining the EEG data and ensuring its suitability for subsequent analysis and interpretation. In this work, we have strictly taken the second half of each EEG trail from each dataset for experimentation to obtain steady emotions by avoiding transient emotions [33].

IV. METHODOLOGY

The major novelty of this work lies in proposing entropy-based features from the time-frequency (T-F) decomposed EEG signals, which help quantify and capture emotion-aware traits of EEG signals effectively. These features eventually lead to precise recognition performance using the GSCV-optimised XGboost classifier. In this work, we investigated two T-F signal analysis tools, CEEMDAN and LMD, to decompose the EEG signals into mode functions, which help us localize emotion-relevant frequency rhythms in the EEG signals. The CEEMDAN is an advanced variant of EMD and is effective in solving issues of EMD and its variants, including mode mixing issues and noisy IMFs. Moreover, LMD is a novel T-F analysis approach for emotion recognition introduced in this work, which is computationally more efficient than EMD variants. This work presented a comparative performance analysis of both the approaches, i.e., CEEMDAN and LMD, by deriving the entropy-based non-linear features from split EEG signals called mode functions such as IMFs and PFs that represent emotion-relevant content quite effectively. The popular machine learning (ML) models are employed to classify the entropy features and select a model that considerably assists in accurately identifying emotions. Fig.1 depicts a schematic flow of the proposed approach, and more details about each T-F analysis approach adopted in this work are discussed in subsequent sections.

A. COMPLETE ENSEMBLE EMPIRICAL MODE DECOMPOSITION WITH ADAPTIVE NOISE (CEEMDAN) OF MULTICHANNEL EEG SIGNALS

The CEEMDAN decomposition defines white Gaussian noise's standard deviation (SD) $GW^i(n)$ (where I = 1, 2, ..., P). P denotes the number of EEG channels, and each channel is decomposed individually and an operator $C_j(.)$ that yields the jth mode of EMD. The decomposition process is demonstrated below step-wise:

1. Obtain $x(n) + \sigma_d GW^i(n)$ by adding P groups of white Gaussian noise $W^i(n)$ to input EEG signals x(n) where i =1,2,3...P.
2. Next, using EMD, compute the first modal component denoted by $IMF_{1,P}$ ($IMF_{1,1}$, $IMF_{1,2}$, $IMF_{1,P}$) of each group of the P number of EEG channels. The average of these first mode functions could be expressed [21] as below:

$$IMF_1(n) = \frac{1}{P}\sum_{i=1}^{P} IMF_1^i(n) = \overline{IMF}_1(n) \tag{1}$$

3. The residue can be computed using the equation below and denoted $\xi_l(n)$

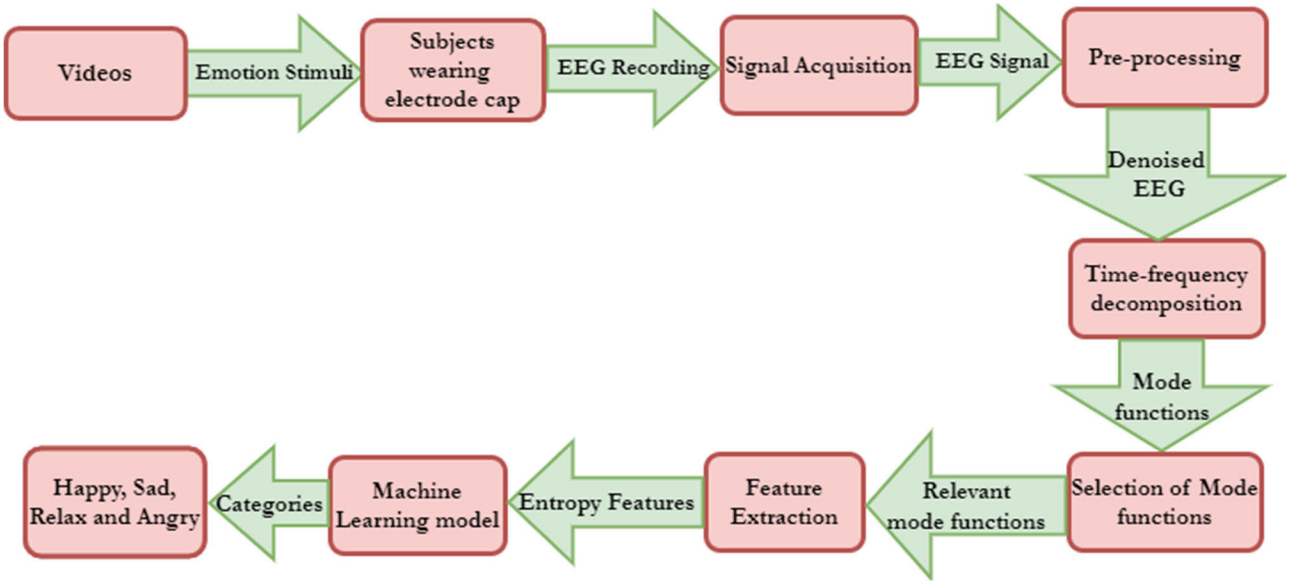

FIGURE 1. A schematic flow diagram of the proposed method.

$$\xi_l(n) = x(n) - IMF_l\,(n) \text{ where } l = 1, 2, 3 \ldots, L \quad (2)$$

The first residue is obtained by substituting l =1, and the equation (2) is transformed as

$$\xi_1(n) = x(n) - IMF_1\,(n) \quad (3)$$

4. The realizations $\xi_1(n) + \sigma_1 c_1\left(GW^i\,(n)\right)$ are divided until their first EMD mode where i=1, 2, 3, 4…, P. σ_l indicate white noise SD of the lth stage (where l=1 for this iteration). The following equation can be used to determine $IMF_2\,(n)$:

$$IMF_2\,(n) = \frac{1}{P}\sum_{i=1}^{P} c_1(\xi_1(n) + \sigma_1 c_1\left(GW^i\,(n)\right) \quad (4)$$

5. Calculate the lth residue for l = 2, 3,…, L.

$$\xi_l(n) = \xi_{l-1}(n) - IMF_l\,(n) \quad (5)$$

6. The realizations $\xi_1(n) + \sigma_1 c_1\left(GW^i\,(n)\right)$ are split till their first mode of EMD, and the (l + 1)th mode is defined as follows.

$$IMF_{l+1}\,(n) = \frac{1}{P}\sum_{i=1}^{P} c_1(\xi_l n) + \sigma_l c_l\left(GW^i\,(n)\right) \quad (6)$$

7. Go back to step 6 to complete the next step. l.
8. As steps 5–7 are repeated, the residue becomes monotonic, and no more modes may be recovered. The convergence criterion is satisfied; no more mode decomposition is achievable if the end residue and l are the maximum number of modes. The input signal x(n) can be recovered from all mode functions of CEEMDAN with the following equation [21]:

$$x(n) = \sum_{l=1}^{L} IMF_l\,(n) + \xi_l(n) \quad (7)$$

B. LOCAL MEAN DECOMPOSITION (LMD) OF THE MULTICHANNEL EEG SIGNALS

This approach offers a robust and analytically simple way of assessing time-varying frequency, energy, and phase in extremely complex non-stationary signals such as EEG. LMD is explored to divide modulated signals into a small number of PFs, while every PF combines an amplitude envelope and frequency-modulated signals [31], [32]. The LMD method produces a physically meaningful EEG time-frequency distribution. Since the frequency components of the EEG (Gamma, alpha, theta, and delta) are related to various mental states, it is feasible to conclude that this method of dividing time-series into various PFs identifiable with their frequency is highly suitable for EEGs [31]. Also, these PFs represent EEG subbands associated with different emotional states in the brain [31]. As a result, we observed LMD to be more appropriate for decomposing the EEG data and applying it to recognize emotions. Using LMD, the EEG signal s(t) is decomposed into PFs [56] as follows:

1. As mentioned below, calculate the local maxima and average score of two nearby maximum data points (n_i and n_{i+1}):

$$z_i = (e_i + e_{i+1})/2 \quad (8)$$

Eq (8), all local means can be represented as straight lines stretching from subsequent extrema. After smoothing the local means via moving averaging, a constantly shifting continual local mean function called $z_{11}(t)$ is produced.

2. By the scenario previously stated, the local magnitude a_i of the two nearby extremes (e_i and e_{i+1}) is expressed [20] by

$$b_i = |e_i + e_{i+1}|/2 \quad (9)$$

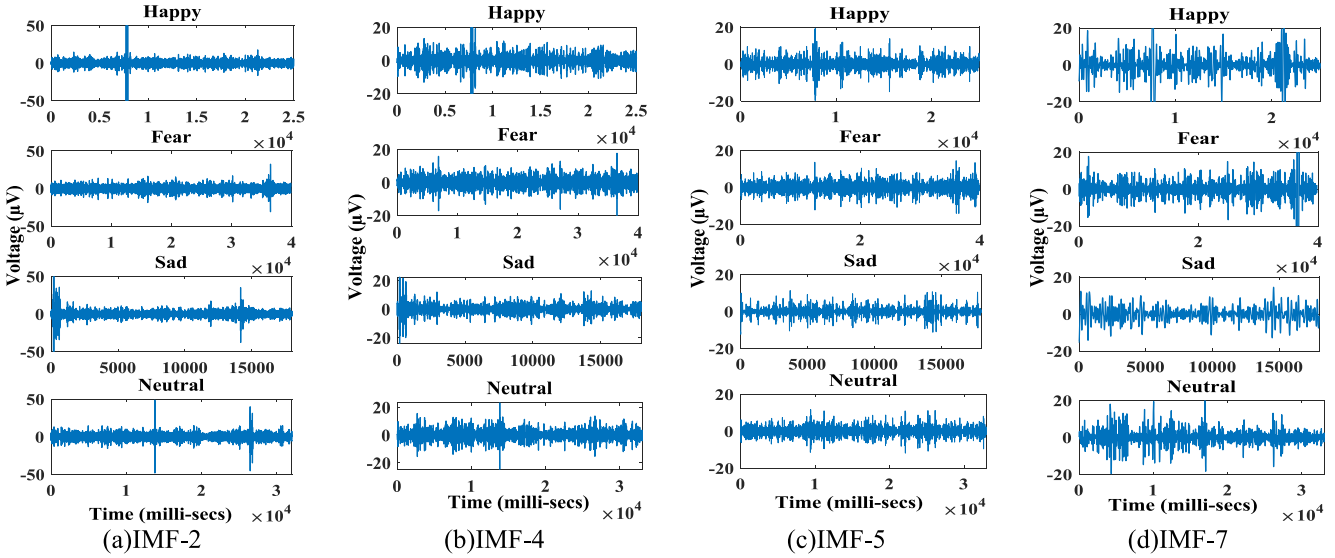

FIGURE 2. Various IMFs obtained after CEEMDAN for four emotion categories of a single participant from the SEED-IV dataset show variations in the amplitudes.

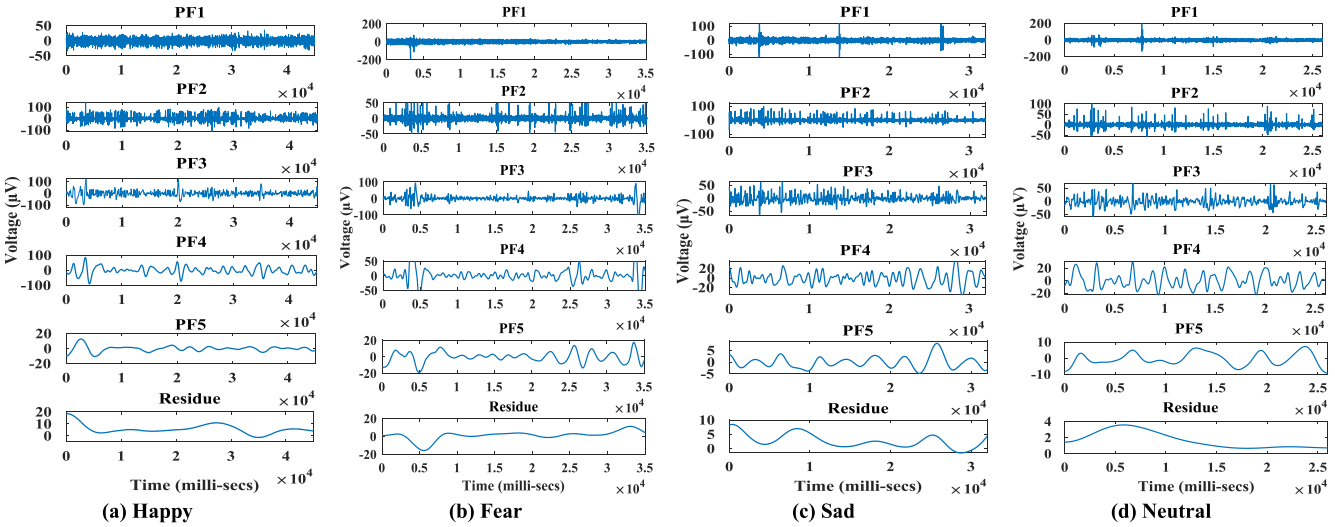

FIGURE 3. Five PFs were obtained after LMD of SEED-IV EEG for four emotions, depicting substantial variations in magnitude and frequency for the four emotion categories.

3. Subtract the local mean function $z_{11}(t)$ [20] from the original EEG signal

$$l_{11}(t) = s(t) - z_{11}(t) \tag{10}$$

Here, the estimated envelope $l_{11}(t)$ is then scaled by $b_{11}(t)$, and demodulated element $d_{11}(t)$ is produced by

$$g_{11}(t) = \frac{s(t) - z_{11}(t)}{b_{11}(t)} = \frac{l_{11}(t)}{b_{11}(t)} \tag{11}$$

4. On the demodulated component, steps 1 through 3 are repeated n times until the EEG signal $g_{1n}(t)$ is ultimately frequency-modulated. A series of recursive equations [20] are produced as a result.

$$\begin{cases} l_{11}(t) = s(t) - z_{11}(t), \\ l_{12}(t) = g_{11}(t) - z_{12}(t), \\ \vdots \\ l_{1n}(t) = g_{1(n-1)}(t) - z_{1n}(t). \end{cases} \tag{12}$$

where

$$\begin{cases} g_{11}(t) = l_{11}(t)/b_{11}(t), \\ g_{12}(t) = l_{12}(t)/b_{12}(t), \\ \vdots \\ g_{1n}(t) = l_{1n}(t)/b_{1n}(t). \end{cases}$$

5. The estimated sub-envelopes are multiplied to create the composite envelope, calculated as:

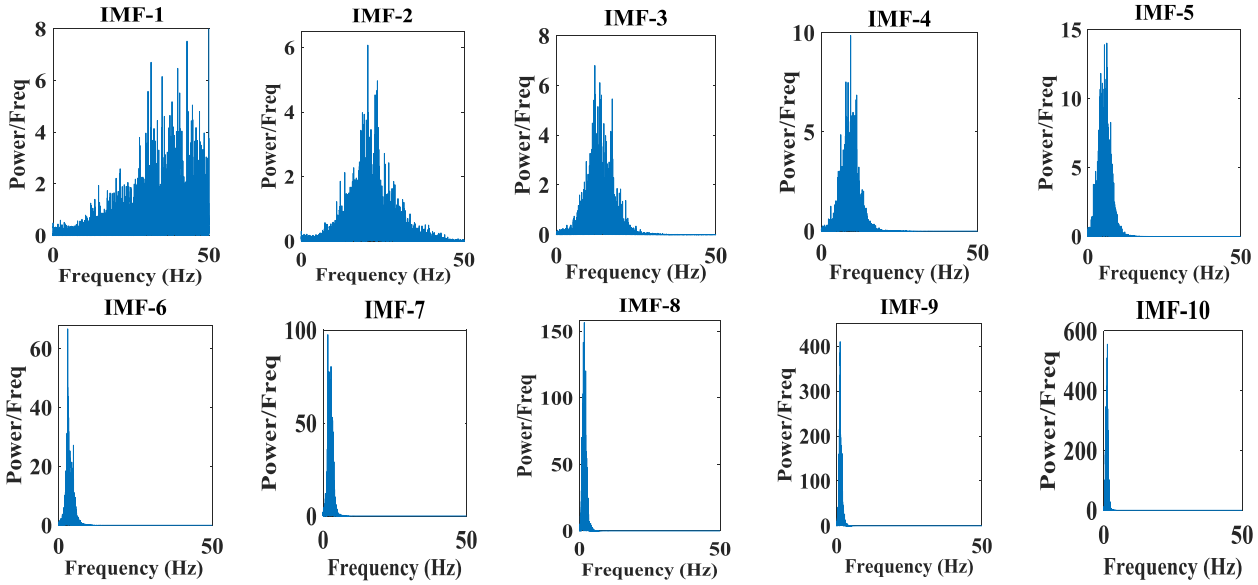

FIGURE 4. Periodograms of the first ten IMFs of a randomly selected EEG signal of SEED IV datasets using the CEEMDAN approach.

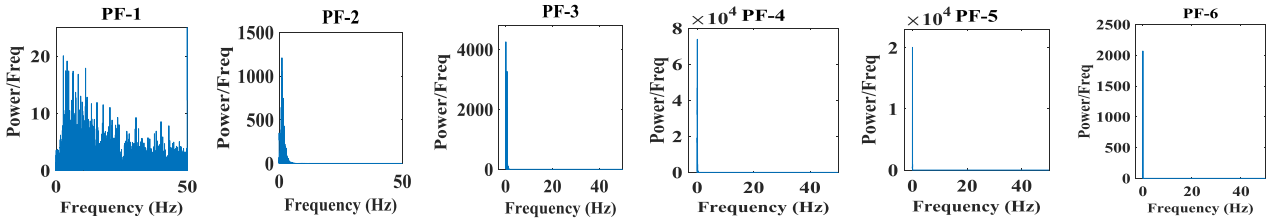

FIGURE 5. Periodograms of the first six PFs of a randomly selected EEG signal of SEED IV datasets of the LMD approach.

$$b_1(t) = b_{11}(t)\, b_{12}(t) \ldots . b_{1n}(t) = \prod_{q=1}^{n} b_{1q}(t) \tag{13}$$

and at last, the aim is to $\lim_{n\to\infty} b_{1n}(t) = 1$.

The first PF1 is produced by multiplying the two functions $g_{1n}(t)$ and $b_{1n}(t)$

$$PF_1(t) = b_1(t)\, g_{1n}(t) \tag{14}$$

6. A signal $r_1(t)$ is obtained by eliminating PF1(t) from s(t)

$$r_1(t) = s(t) - PF_1(t) \tag{15}$$

7. To get the function $r_j(t)$ to become stable and stop oscillating, repeat steps (1) – (5) above j times. This results in EEG input $s(t)$ being divided into j PFs and a residue $r_j(t)$. One can recover the EEG s(t) as

$$s(t) = \sum_{i=1}^{j} PF_i(t) + r_j(t) \tag{16}$$

C. SELECTION OF RELEVANT MODE FUNCTIONS FOR EMOTION RECOGNITION

The T-F analysis of EEG signals through CEEMDAN and LMD techniques has demonstrated their potential for emotion recognition as illustrated by their mode functions, i.e., IMFs and PFs in the previous section for the happy, fear, sad, and neutral emotion classes, as shown in Fig. 2 and 3. It is worth observing that the four emotions of interest exhibit various oscillatory characteristics in terms of their amplitudes and frequencies, as shown in Figs. 2 and 3. Thus, the mode functions carry the discriminating characteristics of each emotion. However, all the mode functions decomposed using CEEMDAN and LMD approaches are irrelevant to their respective EEG signals as the few only represent the dominating EEG rhythms. Hence, selecting relevant mode functions only by discarding the irrelevant ones is essential, which will eventually help reduce the computation burden of the proposed system. We followed a periodogram-based approach to identify the no. of mode functions, capturing the majority of frequency rhythms of the associated EEG. The periodograms of the mode functions are plotted to visualize their power density. Fig. 4 depicts the periodogram plots of the first ten IMFs of EEG signal obtained through the CEEMDAN approach. It is clear from Fig.4 that IMF1-IMF5 periodograms have significant frequency rhythms, which gradually decrease from IMF6- IMF10. Therefore, in a resource-constrained scenario like mobile-based applications, the first five IMFs can only be used as they capture a majority of emotion-relevant EEG variations; however, this study employed IMF1-IMF8 to ensure

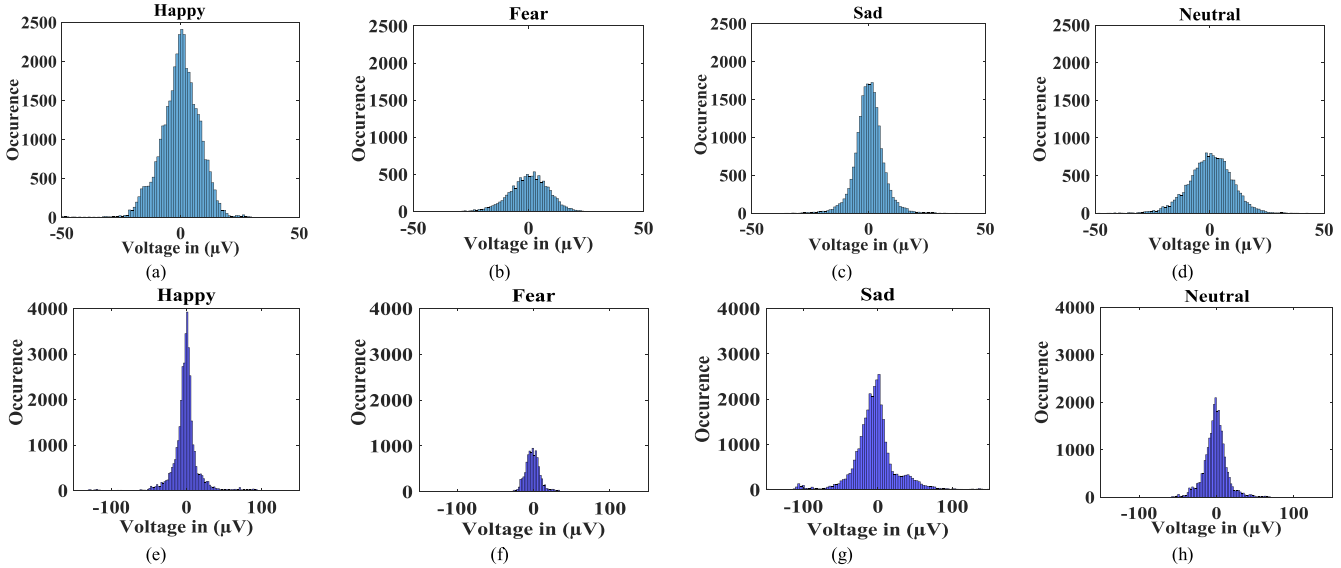

FIGURE 6. (a-d) Histograms of four emotion classes of IMF-3 obtained by CEEMDAN decomposed EEG data from the SEED-IV; and (e-i) histograms of PF-3 obtained by LMD decomposed EEG approach. The distinguishing nature of the histograms can be seen for four emotion classes.

the best performance. Similarly, the periodograms of the first six PFs of an EEG signal obtained through LMD decomposition are plotted in Fig. 5. It can be observed that the PF1-PF3 capture the majority of EEG variations, which might be relevant in capturing different emotions, and minimal frequencies are present in other PFs. Therefore, the first three PFs may be used for computational saving as these represent EEG's dominating emotional power. However, this study used the first five PFs for best recognition results. These relevant mode functions are used for extracting entropy features, which are discussed in detail in the next section.

To further demonstrate the distinguishing capabilities of both categories of mode functions, we plotted the histograms for four emotion classes. As expected, the histogram morphologies show discriminating characteristics for four emotion cases, as seen in Fig. 6. Figs. 6(a-d) are the histograms of IMF-3 obtained through the CEEMDAN decomposition of EEG for four emotions. Similarly, Figs. 6(e-h) are the histograms of PF-3 obtained through LMD decomposition of EEG. It is evident from Fig. 6 that LMD's histograms are more distinguishable than CEEMDAN histograms. Furthermore, the EEG amplitude distributions are distinct, and this difference is directly related to the signal's emotional characteristics varying across four emotion classes.

D. ENTROPY-BASED FEATURE EXTRACTION USING MODE FUNCTIONS

In the previous section, we demonstrated the suitability of CEEMDAN and LMD decomposition for emotion recognition analysis of EEG signals. To further localize the discriminating characteristics of the T-F decomposed EEG (mode functions) for different emotions, we have used entropy features, which help us capture the non-linear characteristics of the mode functions. Entropy is a popular non-linear time series metric employed for EEG signals in many applications [21], [22], [23], such as mental fatigue detection [22], autism analysis [23], and sleep monitoring [21]. This study investigated entropy computations of the T-F decomposed time-series EEG using CEEMDAN and LMD, which may help us overcome the mode-mixing and noise issues of conventional EMD-IMFs. Different types of entropies investigated over the mode functions include approximate, sample, and permutation entropy. For each mode function, the entropy metrics are calculated using the equations described below in detail:

E. Approximate Entropy (ApEn)

ApEn [24] is a regularity statistic that measures the irregularity of mode functions (IMFs and PFs) time series fluctuations. Mathematically, it is calculated using the following expression [24]:

$$ApEn\,(m, r, N) = \ln\left[\frac{X_m\,(r)}{X_{m+1}\,(r)}\right] \tag{17}$$

X_m and X_{m+1} are subsequence mean of length m and m+1, respectively.

F. Sample Entropy (SaEn)

SaEn [24] quantifies the complexity of the IMFs' and PFs' time series. If X^m and X^{m+1} are counters for template vectors of length m and m+1, correspondingly, and computed as below [24]

$$SaEn(m, r, N) = -\ln\left[\frac{X^{m+1}\,(r)}{X^m\,(r)}\right] \tag{18}$$

Here, we have selected m=2 and r=0.2 based on the work [25] for computing the ApEn and SaEn of IMFs and

PFs. The proposed method achieved better performance using these values.

G. Permutation Entropy (PeEn)

PeEn [26] measures the incongruity of the IMFs and PFs time series by computing a smoothened histogram of ordinal patterns seen in subsequences when arranged in ascending order, from which the Shannon entropy is derived. It is calculated with the help of the probability vector of the subsequences as follows [26]:

$$PeEn\,(x, m, N) = -\sum_{k=0}^{m!-1} p_k \log p_k \tag{19}$$

where$m!$ denote the permutations of the pattern length. We have chosen m=5 for our experiments to compute the permutation entropy of EEG-decomposed mode functions [26].

It is generally found that sample entropy is the best choice to discriminate between different groups with the proper selection of the parameters for a time series. For shorter time series, the approximate entropy is inefficient and lacks consistency [24]. Although sample entropy overcomes approximate entropy, the discriminating nature of both entropy measures is highly dependent on the parameter selection. Hence, we investigated bubble entropy (BuEn), a novel entropy measure independent of the parameter selection for feature extraction of mode functions.

H. PROPOSED BUBBLE ENTROPY-BASED FEATURE EXTRACTION IN T-F DOMAIN

BuEn [27] is a significant tool in non-linear dynamics study owing to its potential enhancements upon permutation entropy (PeEn). Its considerable goal is to reduce the entropy metric's dependency on input parameters. Most entropy measures need a minimum of two parameters for their computation: an embedded dimension m and a threshold r. Based on these parameter settings, their performance in discriminating power, artifacts robustness, or any other desirable feature might change. It does not require parameter r, is less volatile on m, and is unbiased for tremendous m values. BuEn places the time-series data, the mode functions of EEG $x=x_1, x_2, x_3\ldots,x_N$ into an m-dimensional space, obtaining a sequence of vectors of dimension N-m+1:

$$X_1, X_2, X_3, \ldots., X_N \tag{20}$$

where $X_j = \{x_j, x_{j+1}, x_{j+2}, \ldots, x_{j+m-1}\}$

The bubble sort technique is implemented to sort every vector Xj, and the number of swaps needed for sorting is recorded. The second-order Renyi entropy is determined using the probability mass function (PMF) p_i of having I swaps:

$$H^m_{swaps} = -\log \sum_{i=0}^{\binom{m}{2}} p_i^2 \tag{21}$$

The BuEn is calculated as the normalized difference of the entropy associated with the swaps required for sorting vectors of lengths m+1 and m:

$$buEn(m) = \left(H^{m+1}_{swaps} - H^m_{swaps}\right) / \log\left(\frac{m+1}{m-1}\right) \tag{22}$$

The vectors Xi are sorted in ascending order; this is merely a practice that has no implications on the classification of the time sequence or the value of BuEn. Similarly, if we consider s^m_j the count of swaps needed to sort the vector X_j in ascending order, then $m(m-1)/2-s^m_j$ sorting steps are necessary to arrange it in descending order. As a result, if pi represents the PMF of the swaps performed for setting all the vectors in ascending order, grouping them in descending produces the PMF $q_j = p_{m(m-1)/2-j}$, resulting in the exact value of H_m swaps in the equation (12). We have considered m=12 for computing the BuEn of IMFs and PFs, as it is clear that the discriminating nature of the BuEn increases for m≥12 [27]. This study experimented with various values of m>12 and found that for m=12, BuEn features obtained a lower p-value, indicating its discriminating power of emotions, as discussed in the next section. It has been noted that ApEn, SaEn, and PeEn suffer from computational challenges and are sensitive to parameter dependencies [24], [25], [26], [27], which motivated us to explore BuEn as a new entropy feature on mode functions that has stable behavior and is independent of the parameters. Moreover, it has a higher potential to study the non-linear dynamics of the given signals. Therefore, we chose BuEn of CEEMDAN and LMD mode functions in most of our experimentation, whose discriminating ability is unbiased with the parameters. Furthermore, we have also computed ApEn, SaEn, and PeEn of mode functions and compared the performance of these entropy techniques with BuEn for the recognition of EEG-based emotions.

I. EEG CHANNEL PROFILING

It is a known fact that not all EEG channels contribute equally to human emotions. Hence, it becomes essential to analyze the contribution of different channels in emotion recognition so that only the relevant EEG channels can be used for emotion recognition tasks while minimizing the computational burden on the emotion detection system. To address this, we performed EEG channel profiling with the following objectives: (i) To reduce the computational complexity of EEG signal processing, we focused on selecting only the significant channels, thereby deriving the essential characteristics; (ii) To handle overfitting issues that may occur due to the use of redundant channels to improve emotion recognition performance, and (iii) To minimize the setup time for building the emotion recognition model. This work considers five different channel profiles as proposed in the study [14] for 62 channels (SEED dataset), and we replicated it for 32 channels (DEAP dataset) following a similar strategy. The emotion recognition performance of all the channel profiles is evaluated. Moreover, a comparative analysis is performed with all EEG channels (62 and 32).

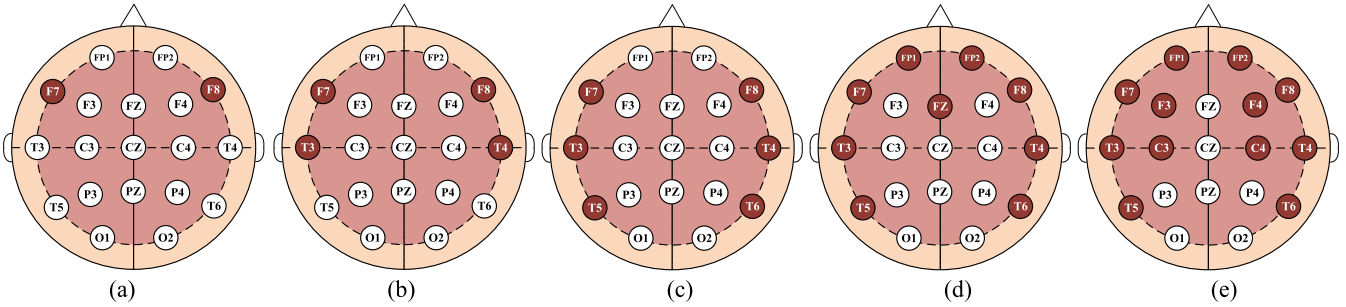

FIGURE 7. Channel selection for (a-e) DEAP dataset respectively.

TABLE 2. Feature matrix dimensions for the various channel profiles of SEED & SEED-IV.

Channel Profile	CEEMDAN approach		LMD approach	
	SEED	SEED-IV	SEED	SEED-IV
2-channel	225×17	360×17	225×11	360×11
4-channel	225×33	360×33	225×21	360×21
6-channel	225×49	360×49	225×31	360×31
9-channel	225×73	360×73	225×46	360×46
12-channel	225×97	360×97	225×61	360×61
All 62-channel	225×497	360×497	225×310	360×310

TABLE 3. Feature matrix dimensions with the two decomposition techniques of the DEAP Dataset.

Channel Profile	Channels selected	CEEMDAN approach	LMD approach
2-channel	F7,F8	1280×17	1280×11
4-channel	F7, F8, T7, and T8	1280×33	1280×21
6-channel	FP1,FP2,F7,F8,T7 and T8	1280×49	1280×31
9-channel	F3,F4, FP1,FP2,F7,F8,T7 and T8	1280×73	1280×46
12-channel	F3,F4,FP1,FP2,F7,F8,FZ, PZ,T3,T4,T7 and T8	1280×97	1280×61
All 32-channel	All 32 channels	1280×497	1280×310

The five different channel profiles analyzed are i) 2-channel, ii) 4-channel, iii) 6-channel, iv) 9-channel, and v) 12-channel, as shown in Table 2 [14], [25]. The authors in [14] proposed these channel profiles considering the channels from the brain's lateral temporal and prefrontal regions. Also, they verified that these regions are highly responsible for emotion processing by computing the weight distribution of these regions using deep belief networks. Moreover, these findings align with their previous studies [52], [53], [54]. Furthermore, it is concluded from [14] that a group of features extracted from the prefrontal and temporal lobes have been identified to provide discriminative information associated with emotion processing. These observations motivated us to use the channel profiles proposed in this study [14]. Thus, we extracted entropy features from these five-channel profiles and all 62 channels to classify emotions. Based on the channel selection strategy reported in [14] for SEED, this work proposed channel selection covering the prefrontal and temporal lobes of the brain and defined five-channel profiles for the DEAP dataset, as shown in Table 3. These channel profiles include i) 2-channel, ii) 4-channel, iii) 6-channel, iv) 9-channel, and vi) 12-channel as shown in Figs. 7(a-e). The EEG signals of these channel profiles are decomposed into mode functions using the two techniques, CEEMDAN and LMD. The length of each mode function is equal to the length of the EEG trial considered for decomposition. Further, different entropy features are computed for each mode function, resulting in an entropy feature matrix. This has resulted in a feature matrix for each channel profile of each dataset. Subsequently, these feature matrices are labeled with the emotion classes available in the respective datasets for classification. As mentioned above, for the 2-channel profile, the feature vector obtained is of dimension $15 \times 15 \times 2 \times (8(\text{or})\ 5)$ (subjects × trails × channels × (IMFs (or) PFs), which leads to the feature matrix of size 225(columns) × 10(rows) for SEED dataset with PFs. Next, the emotion label is appended, resulting in a matrix of dimensions 225 × 11. The same procedure is repeated for each channel profile entropy feature. Table 2 and Table 3 detail the feature matrix dimensions of the two approaches. These extracted features are fed to XGboost to classify different emotion classes.

J. ANALYSIS OF THE DISCRIMINATING CAPABILITIES OF THE ENTROPY FEATURES

Before going to the emotion classification task, it is crucial to demonstrate the discriminating capabilities (ability to identify different emotions) of various proposed entropy features (ApEn, SaEn, PeEn, and BuEn) in the CEEMDAN and LMD domain. This section aims to compare the capabilities of different entropies to localize the emotion-aware traits in other EEG channel profiles. Here, we have calculated the fisher discriminant ratio (F-score) [55] to measure the discriminating power of the entropy features of different channel profiles. The F-score for w^{th} entropy feature vector of a channel profile can be defined [55] as

$$F_w = \frac{\sum_{c=1}^{4}\left(\left(\overline{X}_w^{(c)} - \overline{X}_w\right)^2\right)}{\sum_{c=1}^{4}\left(\frac{1}{n_c-1}\sum_{k=1}^{n_c}\left(\overline{X}_{k,w}^{(c)} - \overline{X}_w\right)^2\right)} \tag{23}$$

TABLE 4. Fisher-scores of entropy features for various channel profiles of the DEAP dataset.

	CEEMDAN approach				LMD approach			
Features	ApEn	SaEn	PeEn	BuEn	ApEn	SaEn	PeEn	BuEn
2-channel	0.0131	0.0149	0.0153	0.0188	0.0152	0.0199	0.0164	0.0210
4-channel	0.0155	0.0202	0.0169	0.0210	0.0169	0.0212	0.0175	0.0233
6-channel	0.0171	0.0280	0.0181	0.0310	0.0182	0.0299	0.0191	0.0325
9-channel	0.0189	0.0289	0.0204	0.0329	0.0197	0.0300	0.0220	0.0352
12-channel	0.0199	0.0321	0.0213	0.0402	0.0217	0.0417	0.0278	0.0422
32-channel	0.0201	0.0403	0.0225	0.0382	0.0228	0.0425	0.0298	0.0443

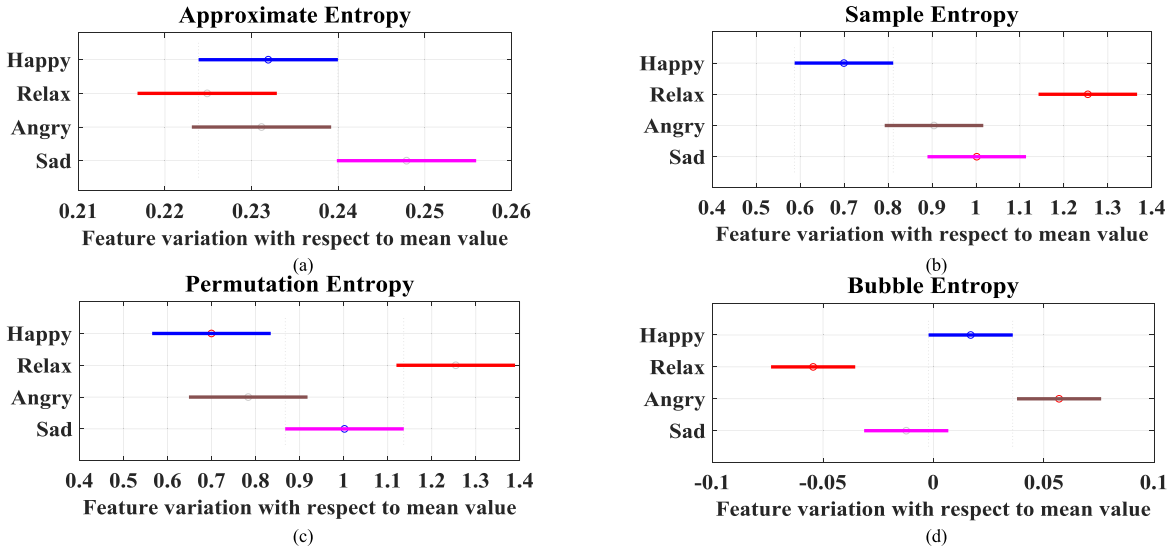

FIGURE 8. The post-hoc analysis of LMD-entropy features with the 12-channel profile of the DEAP dataset.

TABLE 5. ANOVA test probabilistic (p)-value for a 12-channel profile of entropy features.

Entropy	CEEMDAN approach	LMD approach
ApEn	$400000X10^{-8}$	$310000X10^{-8}$
SaEn	$120.4X10^{-8}$	$96.4X10^{-8}$
PeEn	$1.99X10^{-8}$	$1.63X10^{-8}$
BuEn	$3.19X10^{-13}$	$4.14X10^{-14}$

where $\overline{X}_w^{(c)}$ and $\overline{X}_w$ are the average of the features of the emotion category and other emotion categories. $\overline{X}_{k,w}^{(c)}$ are the features of the k^{th} EEG sample of the c^{th} category, and nc denotes the number of samples of the c^{th} category. The Fisher score (F-score) is computed for the entropy features to determine if the estimated values of a quantitative variable differ between feature types. The features that have scored the highest F-score have a good discriminating ability and can be used to classify emotions [35]. The F-score values computed for the four entropy features with every channel profile of the DEAP dataset are depicted in Table 4. It illustrates that CEEMDAN-BuEn and LMD-BuEn features scored higher F-scores than other entropies. This indicates the BuEn features have a higher discriminative power of emotions when compared to other entropy measures. More specifically, the LMD-based BuEn features obtained higher F-scores than CEEMDAN-BuEn features with all channel profiles, as shown in Table 4. This indicates the superior discriminating characteristics of LMD-PFs compared to CEEMDAN-IMFs. This can also be verified from the classification results in the following section. It is also noteworthy to emphasize that the F- score values are very close to each other for all entropy cases of 12-channel and 32-channel profiles, indicating a significant contribution by the 12-channel profile to the EEG's emotional state. To further verify the discriminating ability of BuEn, we have also conducted the statistical analysis, as shown in Fig. 8, using the post-hoc analysis of the ANOVA test. The BuEn feature has minimum overlap across the different emotions compared to all the other entropy features, as shown in Fig. 8, indicating its high discriminative capabilities for various emotions. Moreover, Table 5 details the outcomes of ANOVA test-based discriminative analysis of entropy features in terms of probability (p-value). It can be observed that BuEn has a significantly lower p-value than other entropy measures, indicating its ability to discriminate between different emotions. Furthermore, the LMD-BuEn has a very low p-value compared to CEEMDAN-BuEn features shown in Table 5, indicating a higher discriminating capacity of LMD-BuEn features. Therefore, it can be concluded that BuEn features are the best-performing entropy

TABLE 6. Reported accuracy (%) of the CEEMDAN approach with All-Channel features with various classifiers.

Classifiers	DEAP				SEED				SEED-IV			
	ApEn	SaEn	PeEn	BuEn	ApEn	SaEn	PeEn	BuEn	ApEn	SaEn	PeEn	BuEn
Naive Bayes	63.7	64.2	65.2	76.5	64.7	67.2	67.8	82.5	61.7	64.2	68.2	83.2
ANN	64.8	65.7	67.3	68.3	66.9	67.7	70.3	73.5	63.9	67.7	70.7	74.3
KNN	68.2	68.2	71.3	74.5	69.2	70.2	71.3	79.2	71.2	72.2	73.2	81.3
ELM	72.2	70.3	73.6	80.3	68.2	71.3	75.6	82.3	72.2	74.3	74.3	84.5
LS-SVM	74.9	71.2	73.9	84.5	72.9	73.2	76.2	85.4	75.9	78.2	80.2	82.3
DT	73.2	73.8	75.3	82.3	73.2	73.2	76.8	84.2	77.2	80.2	79.2	83.2
RF	75.2	75.2	76.5	85.2	75.2	75.2	78.5	86.2	78.2	81.2	80.9	87.3
Adaboost	76.7	76.7	76.9	86.7	75.9	75.7	78.9	87.7	78.4	81.9	81.5	88.5
XGboost	78.6	79.1	77.4	88.3	76.6	77.5	80.4	89.4	79.6	83.5	84.5	90.3

TABLE 7. Reported accuracy (%) of the Proposed LMD approach with All-Channel features with various classifiers.

Classifiers	DEAP				SEED				SEED-IV			
	ApEn	SaEn	PeEn	BuEn	ApEn	SaEn	PeEn	BuEn	ApEn	SaEn	PeEn	BuEn
Naive Bayes	65.7	68.2	67.2	70.5	68.7	72.2	67.2	81.8	62.7	68.2	69.2	82.3
ANN	68.9	67.7	68.3	69.5	69.9	76.7	70.3	72.5	64.9	70.7	71.7	76.5
KNN	70.2	73.2	72.3	75.5	72.2	77.2	76.3	80.1	70.2	73.2	74.2	83.2
ELM	74.2	75.3	74.6	81.1	76.2	78.3	79.6	83.5	74.2	77.3	76.3	85.5
LS-SVM	79.9	80.2	81.2	85.5	79.9	80.2	81.2	86.7	77.9	80.2	81.2	84.4
DT	80.2	83.2	82.3	82.9	82.2	84.2	83.3	84.9	79.2	81.2	83.2	84.5
RF	83.2	84.2	84.5	90.7	83.2	85.2	84.5	91.6	81.2	83.2	83.9	93.4
Adaboost	85.6	86.5	85.4	92.3	85.6	87.5	87.4	93.3	84.6	84.5	84.5	94.5
XGboost	86.9	87.2	85.9	93.7	89.9	88.2	88.1	95.2	87.8	89.2	88.2	96.6

features in the LMD domain, with maximum discriminating capability across different emotions. Hence, most of the experiments performed in this study are conducted with BuEn features only.

K. MACHINE LEARNING MODELING FOR EMOTION CLASSIFICATION

After creating a channel-specific feature matrix, the next step is emotion classification. We have examined well-known ML models for classifying entropy features, spanning probabilistic, neural network, distance, and ensemble-based models. It reveals that ensemble-based classifiers perform well. Specifically, the XGboost outperforms all the considered ML models described in the result section. The better classification capability of the conventional XGboost model motivated us to present a grid search cross-validation (GSCV) technique to fine-tune its parameters to enhance its emotion recognition performance further. The following section discusses the experimental results of the conventional XGboost and GSCV-XGboost models in detail.

V. EXPERIMENTAL RESULTS AND ANALYSIS

This section thoroughly evaluates the proposed emotion recognition approach on the aforementioned public databases: DEAP, SEED, and SEED-IV. The cross-validation experiments are performed to analyze the relationship between different channel profiles and their contribution to the brain's emotional states. The three datasets' CEEMDAN and LMD domains entropy features extracted from all-channel profiles are fed to the various classifiers listed in Tables 6 and 7. As per the "no free lunch" theorem [34], no unique optimum classifier exists for a classification task; hence, prominent machine learning classifiers are tested to perform a comparative analysis and select an optimum classifier for our tasks. Tables 6 and 7 compare different classifiers' performance using the discussed entropy traits derived from all EEG channels. Here, the performance of the classifier is measured in terms of accuracy as stated below:

$$\%Accuracy = \text{correct predictions} \big/ \text{total predictions} \quad (24)$$

It reveals that ensemble learning classifiers, such as random forest (RF), Adaboost, and XGboost, keep performing well with all three databases. Moreover, as Tables 6 and 7 reported, BuEn features achieved higher performance than other entropy features. Furthermore, the LMD approach obtained maximum accuracy with all entropy features compared to the CEEMDAN approach. It can be verified from the classification results of XGboost in Table 6 and Table 7 with all the datasets. This shows that LMD-PFs possess a higher discriminating ability for emotions than CEEMDAN-IMFs. However, XGboost outperforms the other classifiers, achieving higher classification accuracy and demonstrating its better suitability in the proposed emotion identification system. Hence, from here on, the XGboost classifier will be used for the rest of the experiments conducted in this work.

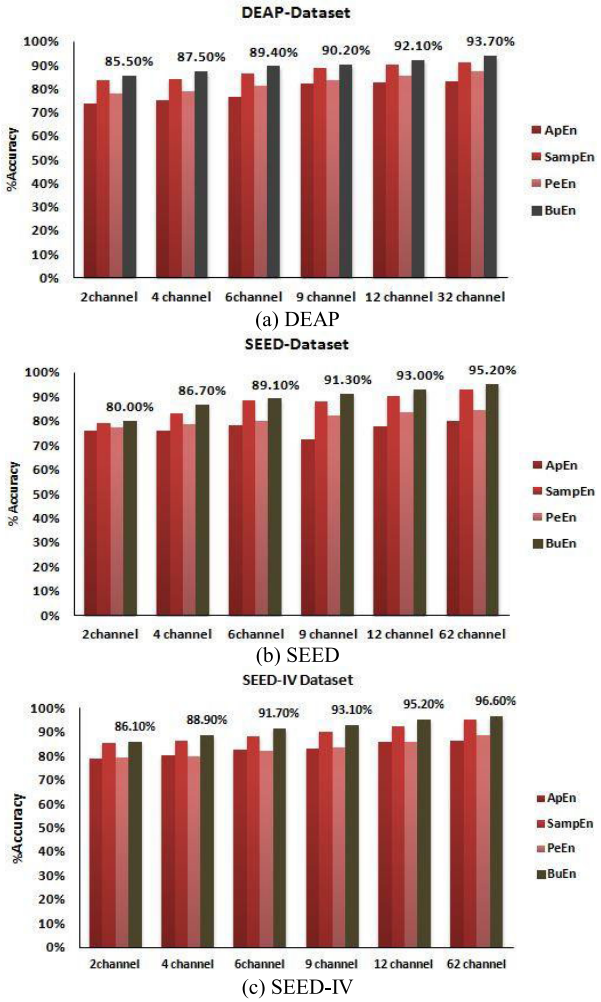

FIGURE 9. Emotion classification performance of various LMD-domain entropies using XGboost.

TABLE 8. ANOVA test probabilistic (p)-value for various channel profiles of BuEn features of the DEAP dataset.

Channel-profile	CEEMDAN approach	LMD approach
2-channel	500000×10^{-8}	710000×10^{-8}
4-channel	130.4×10^{-8}	198.4×10^{-8}
6-channel	1.21×10^{-10}	1.63×10^{-11}
9-channel	3.19×10^{-10}	4.89×10^{-11}
12-channel	2.4×10^{-12}	3.9×10^{-13}
32-channel	3.5×10^{-12}	6.8×10^{-13}

A. ANALYSIS OF CONTRIBUTIONS OF DIFFERENT EEG CHANNEL PROFILES IN EMOTION RECOGNITION

Based on the analysis in the previous section, we can infer that the LMD decomposition followed by BuEn features enabled the XGboost classifier to achieve better performance for the three datasets, as shown in Table 7. Thus, we experimented with XGboost, considering the five channel profiles of LMD-BuEn features of the three datasets to verify the channel profiles' relevancy in emotion classification. The obtained classification accuracy of the channel profiles with the three datasets is depicted in Fig. 9 and compared with all-channel

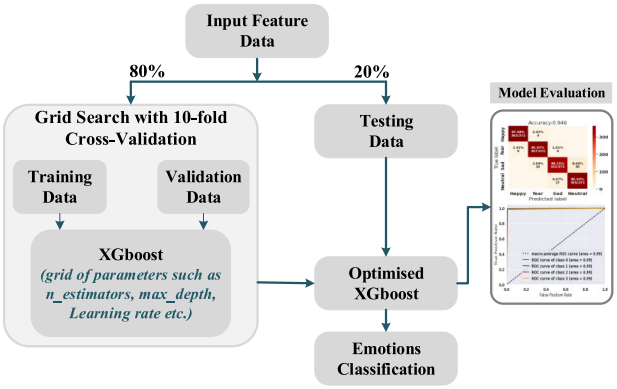

FIGURE 10. Demonstrates the data splitting and GSCV process with XGboost.

profile performances. It is observed that taking all 32 channels of DEAP, the XGboost reported 93.7% accuracy with the LMD approach, as shown in Fig. 9(a), which is marginally higher (1.6%) than the 12-channel profile (92.10%) taken. As the number of EEG channels increases (from 12 to 32), more emotion-relevant information is expected to be added to the classifier, resulting in a better emotion recognition performance (marginal gain of 1.6%). However, this comes at the cost of a significant increase in the computational burden of the system (for processing 32 channels).

Similarly, XGboost reported 95.2% and 96.6% accuracy with SEED and SEED-IV datasets, as depicted in Figs. 9(b-c), respectively, for 12 channel profiles. If we take all 62 channels together, the percentage gain in accuracy is merely 2.2% and 1.4% for the SEED and SEED-IV datasets, respectively, as shown in the comparative figure. This implies that the specific 12-channel combination is responsible mainly for a person's emotional state as it captures almost all the characteristics of EEG required for emotion processing. Therefore, in a resource-constrained scenario, processing the proposed 12-channel profile is much more beneficial compared to 62 channels. It may lead to significant savings in the computational resources at a marginal loss of (1.4-2.2%) in the system's emotion recognition accuracy.

Further, to support our findings about the contribution of different EEG channel profiles to conveying emotional traits, we conducted an ANOVA test with the five-channel profiles using BuEn features. Specifically, it tells us whether there is a statistically significant difference in the means of the five profiles BuEn features. It is clear from Table 8 that all the channel profile features of the two approaches are below the p-value threshold ($p<0.001$). It is observed that the 12-channel profile has a p-value close to the 32-channel profile of shallow values with both the T-F analysis approaches, indicating the effectiveness of the 12-channel combination for emotion processing. Similar statistics were obtained for 12-channel and 62-channel profiles in SEED and SEED-IV datasets. Therefore, after this analysis, we can say that the emotion-relevant contribution of EEG channels from the

TABLE 9. List of Hyper parameters used with XGboost for all channel experiments conducted with DEAP.

Hyper-parameter	Description	Range of values
Learning_rate	To avoid over-fitting, step size shrinkage is used in updates.	0.05,0.5
n_estimators	Number of trees	50,100,150,200,250,300
Max_depth	A tree's maximum depth.	5,6,7,8
Min_child_weight	Lowest sum of instance weight required in a child.	0.01,0.05,0.1
gamma	Lowest loss reduction necessary to create a new division on a tree leaf node.	0.1,0.3,0.5
sub_sample	ratio of the training examples' subsamples.	0.7,1
Col_sample by tree	a variable used in the columns subsampling	0.7,1
reg_lamda	Weights subject to L2 regularisation.	0.4,0.5
reg_alpha	Weights subject to L1 regularisation.	0.01,0.05

TABLE 10. %Classification accuracy obtained by the XGboost and GSCV-XGboost models.

Channel Profile	Model	DEAP	SEED	SEED-IV
12-channel	XGboost	92.10	93.00	95.20
	GSCV-XGboost	94.10	95.60	97.20
All-channels	XGboost	93.70	95.20	96.60
	GSCV-XGboost	95.70	97.80	98.60

prefrontal and temporal lobes is significantly higher than that of other brain regions.

Though the performance of the XGboost was better compared to the state-of-art classifiers, we further presented a fine-tuning approach using the grid search cross-validation (GSCV) technique that tunes the model's parameters for enhanced recognition performance, as discussed in the next section.

B. GRID SEARCH CROSS-VALIDATION (GSCV)-XGBOOST

The most challenging part of machine learning modeling is parameter tuning since decision tree methods are prone to overfitting. Therefore, optimal hyper-tuning of the parameters is necessary to obtain low bias and low variance of the model. In addition to preventing model overfitting on training examples, this would improve precision on unknown test data. We employed the grid search (GS) technique in the Scikit-learn framework [32] on the extracted features to find the best possible set of parameters. At first, we divided the all-channel feature matrices of the three datasets into 80% for training and validation data and 20% for test data, i.e., completely unseen by the model, as shown in Fig. 10. Here, the grid search (GS) with a 10-fold cross-validation (CV) strategy is employed using 80% data. Thus, 80% of the data is portioned into ten subsets, where nine subsets are utilized to train the model per each parameter combination, and the remaining set is used for validation. The process is iterated ten times, taking each group for model validation. We chose the hyper parameters that produced the best accuracy for the CV experiments and utilized those parameter settings to create an optimized XGboost model. Table 9 lists fine-tuned GSCV-XGboost hyper-parameters obtained for the DEAP dataset with all-channel BuEn features. Afterward, the optimized model is evaluated using the 20% test set. A similar GSCV procedure is adopted for 12-channel experiments of the three datasets, and fine-tuned hyper parameters are opted for. Finally, the optimized GSCV-XGboost is evaluated with the test data of 12-channel and all-channel profiles of the three datasets, and the obtained accuracy is reported in Table 10. GSCV-XGboost achieved more than 2% higher accuracy than the conventional XGboost model. Hence, as expected, the grid search optimization of XGboost improved the classification performance. The following section presents these outcomes in terms of the confusion matrix and ROC-AUC values.

C. EVALUATION OF THE PROPOSED METHOD USING GSCV-XGBOOST AND OTHER PERFORMANCE METRICS

We have examined the experimental outcomes of the proposed LMD-BuEn approach using GSCV-XGboost with a variety of other performance metrics too, such as confusion matrices, the receiver operating characteristics (ROC), and area under the curve (AUC), along with accuracy and demonstrated the relevance of these metrics in real-world applications. Since accuracy is not considered a strictly credible indicator for a recognition issue, performance evaluation in the context of additional metrics would help demonstrate the robustness and reliability of the proposed framework.

(i) Confusion matrix (CM): It is a widely used tabular metric that shows the numerical statistics of the model's class-wise classification/miss-classification performance. The percentage discriminating accuracy achieved by the GSCV-XGboost in Table 10 can be verified with the CMs depicted in Fig. 11(b, d, f) for the respective three datasets. Moreover, CM gives insights into the misclassified instances and individual class accuracy. The classification accuracy achieved with test data on conducting cross-validation experiments with XGboost is plotted as CMs. Here, CMs are computed for 12 channels and all channel profiles of each dataset, as shown in Fig. 11. We can observe from Fig. 11(a) that there are only two incorrectly categorized instances of each positive and neutral emotion class of the SEED dataset. Meanwhile, the 62-channel CM has only one incorrectly categorized instance of the positive emotion shown in Fig. 11(b). So, there is only a marginal difference in the misclassification rate of the 12 and all channel profiles, which reinstates that in a resource-constrained scenario, the 12-channel profile is preferable over the 62-channel. Similar observations can be

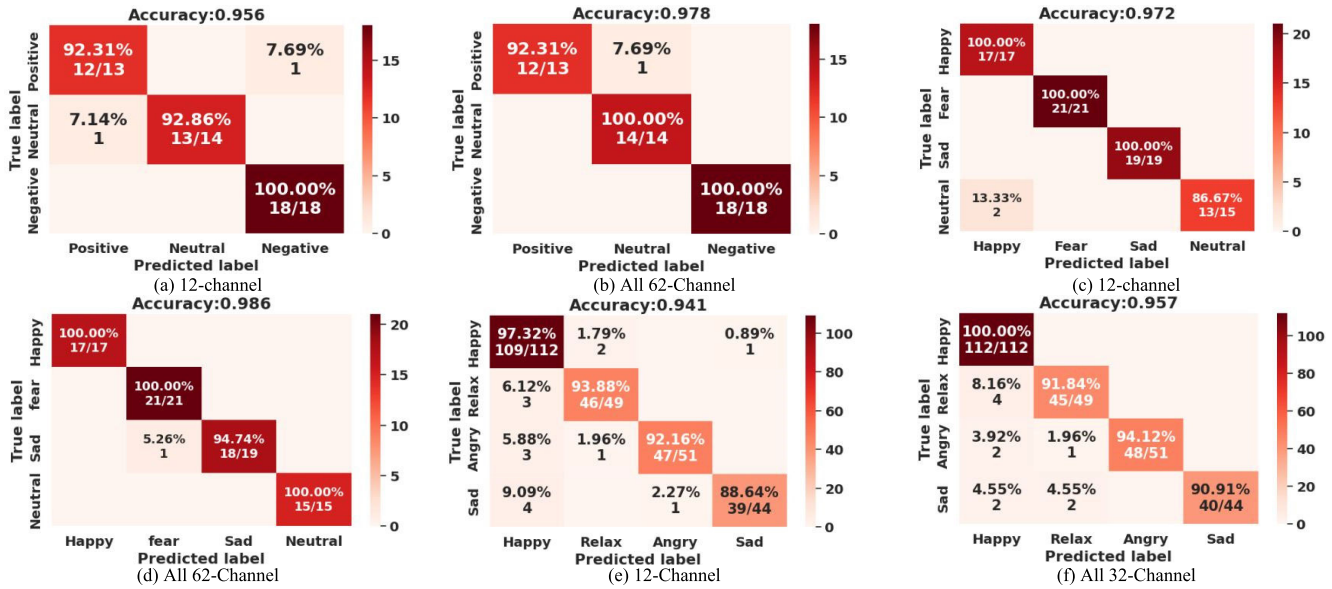

FIGURE 11. Confusion matrices for 12 and all-channel (62 and 32) experiments performed using (a-b) SEED, (c-d) SEED-IV, and (e-f) DEAP datasets.

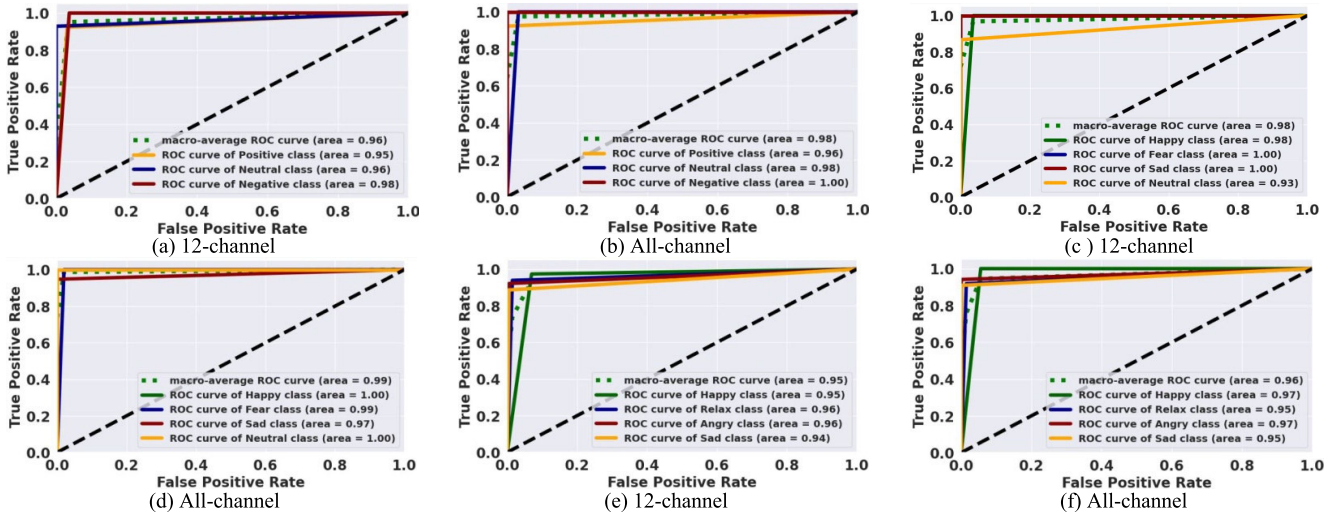

FIGURE 12. ROC curves for 12-channel and All-channel (62 and 32)experiments (a-b) SEED,(c-d) SEED-IV, and (e-f) DEAP datasets.

made from the CMs of the other two datasets, SEED-IV and DEAP, shown in Fig. 11(c-f).

(ii) ROC Curve: It relates true positive rate (TPR) and false positive rate (FPR). Moreover, ''area under the curve (AUC)'' is a crucial parameter that assesses the classifier's efficiency among all viable thresholds and is utilized for classifier evaluation. Therefore, to analyze the XGboost model further, we evaluated the model using a more consistent and effective metric. The ROC curves and AUC values illustrate how well XGboost discriminates between four emotion classes. The ROC is plotted for each dataset's 12-channel and all-channel profiles, shown in Figs. 12(a-f). The most significant outcome of ROC curves was the average AUC obtained with the 12-channel experiments, which are 0.96, 0.98, and 0.95 for the employed datasets, as depicted in Figs. 12(a, c, e). On the other hand, when all channels are considered, AUC values are 0.98, 0.99, and 0.96, which are almost close to 12-channel AUC values for the three datasets shown in Figs. 12(b, d, f). The individual class-level AUC scores are also mentioned in each ROC curve. Hence, the CMs and AUC analysis also confirmed that 12-channel and all-channel profiles performed almost equally well.

D. CROSS SUBJECT VALIDATION (CSV)

CSV experiments are implemented to demonstrate the robustness of the proposed approach. It mainly illustrates the efficacy of the proposed framework in dealing with inter-subject variability, primarily found in real-world HCI applications.

TABLE 11. The classification accuracy of CSV experiments with the three datasets.

Experiments	Dataset	Emotion Category	%ACA
CSV-1	**SEED**	Happy	97.01
		Neutral	96.01
		Sad	96.02
		Average	**96.34**
CSV-2	**SEED-IV**	Happy	97.68
		Fear	94.13
		Sad	95.92
		Neutral	96.21
		Average	**95.98**
CSV-3	**DEAP**	Happy	90.21
		Angry	89.20
		Sad	88.50
		Relax	88.68
		Average	**89.14**

These evaluations are called subject-independent emotion recognition (SIER). This experiment keeps one subject out for testing, and the remaining subjects are fed to the proposed model for training and validation. A similar procedure is followed on every subject, and the test accuracy attained with each subject is averaged to obtain the average classification accuracy (ACA) reported in Table 11. Experiments are performed on three datasets, and the achieved %ACA is summarized in Table 11. The CSV-1 is performed on SEED with three emotions, i.e., happy, neutral, and sad. Further, the CSV-2 is performed with four emotions of SEED-IV. The CSV-3 experiment is executed with DEAP to classify four emotion categories. As depicted in Table 11, observations reveal that the XGboost model obtained superior recognition performance for the three experiments with the proposed T-F domain BuEn features in terms of higher %ACA at individual class and average accuracy levels. For the CSV-1, XGboost attained the maximum 97.01% ACA for the happy emotion class and the minimum for sad 96.02%. Next, with the four-class CSV-2 experiment, the happy class XGboost reported a maximum of 97.68% ACA and a minimum of 94.13% ACA. Further, with CSV-3, the XGboost achieved 89.14% maximum %ACA with a maximum of ACA (90.21%) in the happy emotion class and the minimum for the sad class (88.50%) obtained. In these CSV experiments, XGboost achieved higher accuracy for positive emotions than negative classes. We can conclude from these findings that, even with CSV, accomplished superior results, illustrating its efficacy for SIER tasks.

E. CROSS DATASET VALIDATION (CDV)

Cross-dataset validation is conducted on the SEED and DEAP databases, i.e., we train the model using 90% of the train data from one database and tested on 10% of data from other databases. For this experiment, this work considered only two emotion classes (positive and negative) to maintain compatibility within the databases. The high valence and low valence emotion classes are positive and negative emotions

TABLE 12. The classification accuracy of CDV experiments with the three datasets.

Experiment	Train Database	Test Dataset	Classification %Accuracy	GSCV-XGboost
CDV1	DEAP	SEED	Positive	96.51
			Negative	94.88
			Average	**95.69**
CDV2	SEED	DEAP	Positive	88.22
			Negative	82.71
			Average	**85.46**

of DEAP. Consequently, two experiments (CDV-1 and CDV-2) are performed, and the individual classification accuracies of each emotion class are given in Table 12. The key observations that we can infer from this experiment are that the average emotion detection accuracy is reduced in this case by the XGboost model compared to the previous experiment. However, the proposed model's performance in CDV-1 is still close to CSV-2. As DEAP is an imbalanced dataset, the proposed model achieved a marginal performance of 85.46% for CDV-2. Even with the toughest validation like CDV, the performance of the XGboost with proposed T-F domain BuEn features is better, indicating the model's robustness for real-world scenarios. This aspect is crucial in SIER tasks. The proposed emotion recognition system has real-world applications, such as detecting stress or depression and enabling HCI applications. It involves using a wearable EEG device on the subject's head to record EEG samples, which can be collected remotely. By analyzing these EEG signals through the proposed approach, the person's emotional status can be identified.

VI. COMPARATIVE ANALYSIS

Table 13 presents a comparative analysis of the performance of the proposed method against the latest published works in the field of emotion recognition. This study evaluates the percentage accuracy reported in these recent studies. The comparison highlights that the proposed scheme outperforms most recently published methods. Notably, a recent study [16] employed a combination of Convolutional Neural Networks (CNN) and differential entropy, achieving an accuracy of 90.41% on the SEED dataset. However, using the same SEED database, the suggested approach significantly improves recognizing performance to 97.8% by utilizing BuEn features in the LMD context. Moreover, the presented work outperforms the most recent EMD-based studies [17], [18], which achieved 93.8% of the highest accuracy with DEAP four emotions, while we attained 95.7% for the same classes. This might be due to the EMD's drawbacks, such as its issues with mode mixing, noisy IMFs, and deviating intermediate frequency. Deep learning (DL) techniques are frequently used in modern research in emotion recognition. For comparison with our suggested LMD-domain entropy technique, we also incorporated the recently published complex deep models [15], [28], [29], [30], [37], [40], [41], [42], [43], [45], [46], [57], [58], [59], [60], [61].

TABLE 13. Comparative analysis of the proposed work with existing works.

Feature Extraction	Classification	Datasets used		
		DEAP	SEED	SEED-IV
Differential entropy [16]	CNN	-	90.41%	-
Second-order difference plots [17]	MLP	93.8% (4-class)	-	-
AR model [18]	SVM	86.28% (4-class)	-	-
FAWT [19]	Random Forest	71.43% (4-class)	90.48%	-
Time-domain features [15]	CNN and LSTM	94.17% (2-class)	-	-
Raw EEG [28]	ACRNN	93.55% (2-class)	-	-
Raw EEG [29]	CNN, SAE, and DNN	91.17% (2-class)	96.77%	-
Raw EEG [30]	RACNN	95% (2-class)	-	-
Time-domain characteristics [36]	Rotation forest with SVM	-	93.1%	-
Feature maps [37]	CNN	75.17% (2-class)	73.11%	-
Differential entropy [40]	CNN and LSTM	-	97.16%	-
Raw EEG [41]	Capsule network with an attention mechanism	92.48% (2-classes)	-	-
Time domain and frequency domain features [42]	Caps EEGNet	96.68% (3-classes)	-	-
Modified Stockwell transform features [43]	Inception V3 and SVM	88.6% (4-classes)	94.58%	-
Spatial and spectral features [45]	ACTNN	-	98.47%	91.9%
Power topographic maps and temporal statistics [46]	Spatial-temporal feature fusion neural network (STFFNN)	85.8% (2-classes)	-	-
Channel correlation loss [57]	Hierarchical self attention network	71.53% (2-class)	79.5%	-
Raw EEG [58]	Neural Architecture Search(NAS)	97.8% 2-class	-	-
Augmented EEG samples [59]	Generative adversial network	89.74% (4-class)	-	-
Raw EEG [60]	Neural Architecture Search (NAS)	-	74.21%	77.01%
Raw EEG [61]	Progressive graph convolution network (PGCN)	-	-	76.96%
Proposed method: CEEDMAN approach	GSCV-XGboost (12-channel)	88.9% (4-class)	90.7%	91.2%
	GSCV-XGboost (All-channel)	91.2% (4-class)	93.1%	93.9%
Proposed method: LMD approach	GSCV-XGboost (12-channel)	94.1% (4-class)	95.6%	97.2%
	GSCV-XGboost (All-channel)	95.70% (4-class)	97.80%	98.6%

The comparison table demonstrates that the GSCV-optimized XGboost classifier outperforms deep learning (DL) methods in emotion classification by leveraging LMD-domain BuEn features. This superior performance might be attributed to the ensemble nature of XGboost, its extensive parameter tuning capabilities, built-in capacity to handle missing values, and numerous other features. These aspects enable XGboost to make more precise predictions than single classifiers like SVM [18] and DL models. Moreover, the computational cost of DL-based methods is high, often requiring a GPU for training. Additionally, deep models are data-hungry; thus, DL-based research [28], [30], [41] utilized vast amounts of raw EEG data. Several studies also employed a wider variety of features [15], [37], [42], [45], [46]. In addition, these studies utilize numerous data processing stages and employ hybrid deep models [15], [28], [29], [30], [41], [42], [43], [45], [46] to distinguish emotions. While experimenting with light ML classifiers and employing only BuEn features in our work, we observed that XGboost performed better than others. Finally, we optimized the parameters of XGboost using the GSCV methodology, fine-tuning aspects such as the number of estimators, maximum depth, and learning rate. This optimization enhanced the discriminative power of XGboost, enabling it to achieve a higher classification rate than recent studies. To the best of our knowledge, the most current DL-based works [42] obtained the highest accuracy with DEAP 96.68% for 3-emotion classes and [45] with SEED (98.47%). Meanwhile, [45] obtained only a marginal accuracy of 91.9% with SEED-IV compared to our LMD approach accuracy of 98.6%. Despite achieving high accuracy [42], it involves many stages for the task, such as the Relief algorithm for channel selection, max-relevance, and min-redundancy algorithm to obtain emotion-relevant channels further and designed capsule EEGNet for emotion recognition. Moreover, [45] also used a hybrid model, i.e., ACTNN, with a complex feature extraction process, i.e., a combination of the spatial feature made into a 2D matrix and spectral characteristics of EEG frequency rhythms. However, the suggested LMD technique exceeds the abovementioned work by attaining the highest accuracy with SEED, SEED-IV, and DEAP, respectively, of 97.8%, 98.6%, and 95.7% without involving complicated procedures. Considering only 12 channels, the proposed LMD method gets competitive performance with SEED and SEED-IV. It achieves superior performance of 94.1% with DEAP, which is particularly noteworthy as it involves four distinct emotion classes. The comparative study suggests that the proposed strategy outperforms existing approaches while requiring reduced computational effort. The BuEn features in the LMD domain adeptly capture emotion-specific characteristics from the EEG signal. In addition, the tuning of hyperparameters in XGboost contributed to enhanced classification. Consequently, the presented method surpassed the overall performance of the previous studies across all three databases. Here, we have also compared our two T-F approaches and found that the LMD approach performs better than the CEEMDAN approach, which might be due to the reason that LMD-domain PFs capture emotion-relevant

traits more precisely from the associated EEG signal as compared to CEEMDAN-domain IMFs. Additionally, the LMD approach was computationally faster than the CEEMDAN approach.

VII. CONCLUSION

This study introduces a novel framework for emotion recognition using a Local Mean Decomposition (LMD) approach to analyze multichannel EEG signals. LMD decomposes EEG signals into product functions (PFs), from which essential mode functions are selected for emotion analysis. The BuEn features are then derived from these functions and fed into an optimized XGboost classifier to distinguish emotions. The F-score and post-hoc analysis revealed that BuEn features have better-discriminating ability than other T-F domain entropy measures. Thus, the BuEn method outperformed other entropy techniques in capturing emotion-relevant information from T-F decomposed EEG signals. Additionally, a channel selection strategy was also proposed to identify the contributions of specific EEG channels in emotion recognition tasks. The 12-channel LMD-BuEn profile significantly improved emotion recognition performance using a GSCV-optimized XGboost classifier. The proposed model, leveraging multichannel LMD-BuEn features, outperformed state-of-the-art methods and proved superior, less complex, and faster than conventional EMD and deep learning-based approaches. The BuEn features from selected EEG channels enhanced the classifier's performance, demonstrated through CSV and CDV experiments. The classification accuracy obtained with the XGboost model for CSV experiments is 96.34%, 95.98%, and 89.14% with SEED, SEED-IV, and DEAP. While with CDV, the results are 95.6% and 85.46% with SEED and DEAP, respectively. Furthermore, the proposed framework's robust performance and low computational demands make it suitable for practical HCI applications, offering superior emotion classification performance. The proposed automatic emotion recognition system can be extended further to be particularly useful in detecting negative emotions like anxiety, stress, and depression, which are critical as they may lead to suicidal tendencies and vary significantly among individuals.

REFERENCES

[1] C. A. Kothe and S. Makeig, "Estimation of task workload from EEG data: New and current tools and perspectives," in *Proc. Annu. Int. Conf. IEEE Eng. Med. Biol. Soc.*, Aug. 2011, pp. 6547–6551.

[2] L. C. Shi and B. L. Lu, "EEG-based vigilance estimation using extreme learning machines," *Neurocomputing*, vol. 102, pp. 135–143, Jul. 2013.

[3] M. Soleymani, M. Pantic, and T. Pun, "Multimodal emotion recognition in response to videos," *IEEE Trans. Affect. Comput.*, vol. 3, no. 2, pp. 211–223, Apr. 2012.

[4] R. A. Calvo and S. D'Mello, "Affect detection: An interdisciplinary review of models, methods, and their applications," *IEEE Trans. Affect. Comput.*, vol. 1, no. 1, pp. 18–37, Jan. 2010.

[5] H. P. Martinez, Y. Bengio, and G. N. Yannakakis, "Learning deep physiological models of affect," *IEEE Comput. Intell. Mag.*, vol. 8, no. 2, pp. 20–33, May 2013.

[6] G. L. Ahern and G. E. Schwartz, "Differential lateralization for positive and negative emotion in the human brain: EEG spectral analysis," *Neuropsychologia*, vol. 23, no. 6, pp. 745–755, Jan. 1985.

[7] S. B. Wankhade and D. D. Doye, "Hybrid hunt-based deep convolutional neural network for emotion recognition using EEG signals," *Comput. Methods Biomechanics Biomed. Eng.*, vol. 25, no. 12, pp. 1311–1331, Sep. 2022.

[8] F. P. Akbulut, "Hybrid deep convolutional model-based emotion recognition using multiple physiological signals," *Comput. Methods Biomechanics Biomed. Eng.*, vol. 25, no. 15, pp. 1678–1690, Nov. 2022.

[9] F. Sauvet, C. Bougard, M. Coroenne, L. Lely, P. Van Beers, M. Elbaz, M. Guillard, D. Léger, and M. Chennaoui, "In-flight automatic detection of vigilance states using a single EEG channel," *IEEE Trans. Biomed. Eng.*, vol. 61, no. 12, pp. 2840–2847, Dec. 2014.

[10] M. Jianbiao, W. Xinzui, L. Zhaobo, L. Juan, Z. Zhongwei, and F. Hui, "EEG signal classification of tinnitus based on SVM and sample entropy," *Comput. Methods Biomechanics Biomed. Eng.*, vol. 26, no. 5, pp. 580–594, Apr. 2023.

[11] J. van Erp, F. Lotte, and M. Tangermann, "Brain-computer interfaces: Beyond medical applications," *Computer*, vol. 45, no. 4, pp. 26–34, Apr. 2012.

[12] M. Paluš, "Nonlinearity in normal human EEG: Cycles, temporal asymmetry, nonstationarity and randomness, not chaos," *Biol. Cybern.*, vol. 75, no. 5, pp. 389–396, Dec. 1996.

[13] A. Mert and A. Akan, "Emotion recognition from EEG signals by using multivariate empirical mode decomposition," *Pattern Anal. Appl.*, vol. 21, no. 1, pp. 81–89, Feb. 2018.

[14] W.-L. Zheng and B.-L. Lu, "Investigating critical frequency bands and channels for EEG-based emotion recognition with deep neural networks," *IEEE Trans. Auto. Mental Develop.*, vol. 7, no. 3, pp. 162–175, Sep. 2015.

[15] Y. Zhang, J. Chen, J. H. Tan, Y. Chen, Y. Chen, D. Li, and W. Che, "An investigation of deep learning models for EEG-based emotion recognition," *Frontiers Neurosci.*, vol. 14, May 2020, Art. no. 622759.

[16] S. Hwang, K. Hong, G. Son, and H. Byun, "Learning CNN features from DE features for EEG-based emotion recognition," *Pattern Anal. Appl.*, vol. 23, no. 3, pp. 1323–1335, Aug. 2020.

[17] N. Salankar, P. Mishra, and L. Garg, "Emotion recognition from EEG signals using empirical mode decomposition and second-order difference plot," *Biomed. Signal Process. Control*, vol. 65, Mar. 2021, Art. no. 102389.

[18] Y. Zhang, S. Zhang, and X. Ji, "EEG-based classification of emotions using empirical mode decomposition and autoregressive model," *Multimedia Tools Appl.*, vol. 77, no. 20, pp. 26697–26710, Oct. 2018.

[19] V. Gupta, M. D. Chopda, and R. B. Pachori, "Cross-subject emotion recognition using flexible analytic wavelet transform from EEG signals," *IEEE Sensors J.*, vol. 19, no. 6, pp. 2266–2274, Mar. 2019.

[20] Y. Wang, Z. He, and Y. Zi, "A comparative study on the local mean decomposition and empirical mode decomposition and their applications to rotating machinery health diagnosis," *J. Vibrat. Acoust.*, vol. 132, no. 2, pp. 1–10, Apr. 2010.

[21] A. R. Hassan and M. I. H. Bhuiyan, "Computer-aided sleep staging using complete ensemble empirical mode decomposition with adaptive noise and bootstrap aggregating," *Biomed. Signal Process. Control*, vol. 24, pp. 1–10, Feb. 2016.

[22] C. Zhang, L. Sun, F. Cong, and T. Ristaniemi, "Spatiotemporal dynamical analysis of brain activity during mental fatigue process," *IEEE Trans. Cognit. Develop. Syst.*, vol. 13, no. 3, pp. 593–606, Sep. 2021.

[23] B. A. Cociu, S. Das, L. Billeci, W. Jamal, K. Maharatna, S. Calderoni, A. Narzisi, and F. Muratori, "Multimodal functional and structural brain connectivity analysis in autism: A preliminary integrated approach with EEG, fMRI, and DTI," *IEEE Trans. Cognit. Develop. Syst.*, vol. 10, no. 2, pp. 213–226, Jun. 2018.

[24] L. Montesinos, R. Castaldo, and L. Pecchia, "On the use of approximate entropy and sample entropy with centre of pressure time-series," *J. NeuroEngineering Rehabil.*, vol. 15, no. 1, pp. 1–15, Dec. 2018.

[25] Y. Zhang, X. Ji, and S. Zhang, "An approach to EEG-based emotion recognition using combined feature extraction method," *Neurosci. Lett.*, vol. 633, pp. 152–157, Oct. 2016.

[26] A. Martínez-Rodrigo, B. García-Martínez, L. Zunino, R. Alcaraz, and A. Fernández-Caballero, "Multi-lag analysis of symbolic entropies on EEG recordings for distress recognition," *Frontiers Neuroinform.*, vol. 13, pp. 1–15, Jun. 2019.

[27] G. Manis, M. Aktaruzzaman, and R. Sassi, "Bubble entropy: An entropy almost free of parameters," *IEEE Trans. Biomed. Eng.*, vol. 64, no. 11, pp. 2711–2718, Nov. 2017.

[28] W. Tao, C. Li, R. Song, J. Cheng, Y. Liu, F. Wan, and X. Chen, "EEG-based emotion recognition via channel-wise attention and self attention," *IEEE Trans. Affect. Comput.*, vol. 14, no. 1, pp. 382–393, Jan. 2023.
[29] J. Liu, G. Wu, Y. Luo, S. Qiu, S. Yang, W. Li, and Y. Bi, "EEG-based emotion classification using a deep neural network and sparse autoencoder," *Frontiers Syst. Neurosci.*, vol. 14, pp. 1–14, Sep. 2020.
[30] H. Cui, A. Liu, X. Zhang, X. Chen, K. Wang, and X. Chen, "EEG-based emotion recognition using an end-to-end regional-asymmetric convolutional neural network," *Knowledge-Based Syst.*, vol. 205, Oct. 2020, Art. no. 106243.
[31] J. S. Smith, "The local mean decomposition and its application to EEG perception data," *J. Roy. Soc. Interface*, vol. 2, no. 5, pp. 443–454, Dec. 2005.
[32] T. Zhang and W. Chen, "LMD based features for the automatic seizure detection of EEG signals using SVM," *IEEE Trans. Neural Syst. Rehabil. Eng.*, vol. 25, no. 8, pp. 1100–1108, Aug. 2017.
[33] N. Pusarla, A. Singh, and S. Tripathi, "Learning DenseNet features from EEG based spectrograms for subject independent emotion recognition," *Biomed. Signal Process. Control*, vol. 74, Apr. 2022, Art. no. 103485.
[34] D. H. Wolpert, "The lack of a priori distinctions between learning algorithms," *Neural Comput.*, vol. 8, no. 7, pp. 1341–1390, Oct. 1996.
[35] C. Godin, F. Prost-Boucle, A. Campagne, S. Charbonnier, S. Bonnet, and A. Vidal, "Selection of the most relevant physiological features for classifying emotion," *Emotion*, vol. 40, no. 20, 2015.
[36] A. Subasi, T. Tuncer, S. Dogan, D. Tanko, and U. Sakoglu, "EEG-based emotion recognition using tunable Q wavelet transform and rotation forest ensemble classifier," *Biomed. Signal Process. Control*, vol. 68, Jul. 2021, Art. no. 102648.
[37] A. Topic and M. Russo, "Emotion recognition based on EEG feature maps through deep learning network," *Eng. Sci. Technol., Int. J.*, vol. 24, no. 6, pp. 1442–1454, Dec. 2021.
[38] Y. Freund and R. E. Schapire, "A decision-theoretic generalization of on-line learning and an application to boosting," *J. Comput. Syst. Sci.*, vol. 55, no. 1, pp. 119–139, Aug. 1997.
[39] R. Sharma, R. B. Pachori, and P. Sircar, "Automated emotion recognition based on higher order statistics and deep learning algorithm," *Biomed. Signal Process. Control*, vol. 58, Apr. 2020, Art. no. 101867.
[40] A. Iyer, S. S. Das, R. Teotia, S. Maheshwari, and R. R. Sharma, "CNN and LSTM based ensemble learning for human emotion recognition using EEG recordings," *Multimedia Tools Appl.*, vol. 82, no. 4, pp. 4883–4896, Feb. 2023.
[41] S. Liu, Z. Wang, Y. An, J. Zhao, Y. Zhao, and Y.-D. Zhang, "EEG emotion recognition based on the attention mechanism and pre-trained convolution capsule network," *Knowl.-Based Syst.*, vol. 265, Apr. 2023, Art. no. 110372.
[42] K. Chen, H. Jing, Q. Liu, Q. Ai, and L. Ma, "A novel caps-EEGNet combined with channel selection for EEG-based emotion recognition," *Biomed. Signal Process. Control*, vol. 86, Sep. 2023, Art. no. 105312.
[43] B. Zali-Vargahan, A. Charmin, H. Kalbkhani, and S. Barghandan, "Deep time-frequency features and semi-supervised dimension reduction for subject-independent emotion recognition from multi-channel EEG signals," *Biomed. Signal Process. Control*, vol. 85, Aug. 2023, Art. no. 104806.
[44] N. Kouka, R. Fourati, R. Fdhila, P. Siarry, and A. M. Alimi, "EEG channel selection-based binary particle swarm optimization with recurrent convolutional autoencoder for emotion recognition," *Biomed. Signal Process. Control*, vol. 84, Jul. 2023, Art. no. 104783.
[45] L. Gong, M. Li, T. Zhang, and W. Chen, "EEG emotion recognition using attention-based convolutional transformer neural network," *Biomed. Signal Process. Control*, vol. 84, Jul. 2023, Art. no. 104835.
[46] Z. Wang, Y. Wang, J. Zhang, C. Hu, Z. Yin, and Y. Song, "Spatial–temporal feature fusion neural network for EEG-based emotion recognition," *IEEE Trans. Instrum. Meas.*, vol. 71, pp. 1–12, 2022.
[47] K. Barnova, R. Martinek, R. Jaros, R. Kahankova, K. Behbehani, and V. Snasel, "System for adaptive extraction of non-invasive fetal electrocardiogram," *Appl. Soft Comput.*, vol. 113, Dec. 2021, Art. no. 107940.
[48] W.-L. Zheng, W. Liu, Y. Lu, B.-L. Lu, and A. Cichocki, "EmotionMeter: A multimodal framework for recognizing human emotions," *IEEE Trans. Cybern.*, vol. 49, no. 3, pp. 1110–1122, Mar. 2019.
[49] S. Koelstra, C. Muhl, M. Soleymani, J.-S. Lee, A. Yazdani, T. Ebrahimi, T. Pun, A. Nijholt, and I. Patras, "DEAP: A database for emotion analysis ;Using physiological signals," *IEEE Trans. Affect. Comput.*, vol. 3, no. 1, pp. 18–31, Jan. 2012.
[50] V. J. Lawhern, A. J. Solon, N. R. Waytowich, S. M. Gordon, C. P. Hung, and B. J. Lance, "EEGNet: A compact convolutional neural network for EEG-based brain–computer interfaces," *J. Neural Eng.*, vol. 15, no. 5, Oct. 2018, Art. no. 056013.
[51] A. Ayenu-Prah and N. Attoh-Okine, "A criterion for selecting relevant intrinsic mode functions in empirical mode decomposition," *Adv. Adapt. Data Anal.*, vol. 2, no. 1, pp. 1–24, Jan. 2010.
[52] W. J. Ray and H. W. Cole, "EEG alpha activity reflects attentional demands, and beta activity reflects emotional and cognitive processes," *Science*, vol. 228, no. 4700, pp. 750–752, May 1985.
[53] M. Balconi and C. Lucchiari, "Consciousness and arousal effects on emotional face processing as revealed by brain oscillations. A gamma band analysis," *Int. J. Psychophysiology*, vol. 67, no. 1, pp. 41–46, Jan. 2008.
[54] Y.-P. Lin, C.-H. Wang, T.-P. Jung, T.-L. Wu, S.-K. Jeng, J.-R. Duann, and J.-H. Chen, "EEG-based emotion recognition in music listening," *IEEE Trans. Biomed. Eng.*, vol. 57, no. 7, pp. 1798–1806, Jul. 2010.
[55] C. Zhao, C. Li, J. Chao, T. Wang, C. Lei, J. Liu, and H. Peng, "F-score based EEG channel selection methods for emotion recognition," in *Proc. IEEE Int. Conf. E-Health Netw., Appl. Services (HEALTHCOM)*, Mar. 2021, pp. 1–6.
[56] N. Pusarla, A. Singh, and S. Tripathi, "Normal inverse Gaussian features for EEG-based automatic emotion recognition," *IEEE Trans. Instrum. Meas.*, vol. 71, pp. 1–11, 2022.
[57] Y. Zhang, H. Liu, D. Zhang, X. Chen, T. Qin, and Q. Zheng, "EEG-based emotion recognition with emotion localization via hierarchical self-attention," *IEEE Trans. Affect. Comput.*, vol. 14, no. 3, pp. 2458–2469, Jul. 2022.
[58] C. Li, Z. Zhang, R. Song, J. Cheng, Y. Liu, and X. Chen, "EEG-based emotion recognition via neural architecture search," *IEEE Trans. Affect. Comput.*, vol. 14, no. 2, pp. 957–968, Apr. 2023.
[59] Z. Zhang, S.-H. Zhong, and Y. Liu, "GANSER: A self-supervised data augmentation framework for EEG-based emotion recognition," *IEEE Trans. Affect. Comput.*, vol. 14, no. 3, pp. 2048–2063, Oct. 2022.
[60] Y. Duan, Z. Wang, Y. Li, J. Tang, Y.-K. Wang, and C.-T. Lin, "Cross task neural architecture search for EEG signal recognition," *Neurocomputing*, vol. 545, Aug. 2023, Art. no. 126260.
[61] Y. Zhou, F. Li, Y. Li, Y. Ji, G. Shi, W. Zheng, L. Zhang, Y. Chen, and R. Cheng, "Progressive graph convolution network for EEG emotion recognition," *Neurocomputing*, vol. 544, Aug. 2023, Art. no. 126262.
[62] Y. Li, S. Zhang, L. Liang, and Q. Ding, "Multivariate multiscale Higuchi fractal dimension and its application to mechanical signals," *Fractal Fractional*, vol. 8, no. 1, p. 56, Jan. 2024.
[63] Y. Li, S. Jiao, S. Deng, B. Geng, and Y. Li, "Refined composite variable-step multiscale multimapping dispersion entropy: A nonlinear dynamical index," *Nonlinear Dyn.*, vol. 112, no. 3, pp. 2119–2137, Feb. 2024.
[64] Y. Li, B. Tang, S. Jiao, and Q. Su, "Snake optimization-based variable-step multiscale single threshold slope entropy for complexity analysis of signals," *IEEE Trans. Instrum. Meas.*, vol. 72, pp. 1–13, 2023.

NALINI PUSARLA received the B.E. degree in electronics and communications engineering from Andhra University, Visakhapatnam, Andhra Pradesh, India, in 2008, and the M.Tech. degree from Jawaharlal Nehru Technological University, Kakinada, India, in 2013. She is currently pursuing the Ph.D. degree with the International Institute of Information and Technology, Naya Raipur, Naya Raipur, India. Her current research interests include biomedical signal processing, machine learning, and deep learning.

ANURAG SINGH (Member, IEEE) received the B.Tech. degree in electronics and communication engineering from Mahatma Jyotiba Phule Rohilkhand University, Bareilly, India, in 2009, the M.Tech. degree in electronics and communication engineering from Indian Institute of Information Technology, Design and Manufacturing, Jabalpur, India, in 2012, and the Ph.D. degree in biomedical signal processing from Indian Institute of Technology Guwahati, Guwahati, India, in 2017. He is currently an Assistant Professor with the Electronics and Communication Engineering Department, International Institute of Information Technology Naya Raipur (IIIT-NR), Atal Nagar-Naya Raipur, India. Prior to joining IIIT-NR, he has been associated as a Faculty Member with the Malaviya National Institute of Technology (MNIT) Jaipur, Jaipur, India, and Thapar University, Patiala, Punjab, India. He was a part of the delegation for the Indo-Japan Student Exchange Program JENESYS-2011. He has published several articles in journals and conference proceedings of international repute. His research interests include machine learning, AI and IoT in healthcare, biomedical signal and image processing, and brain–computer interfacing (BCI). He has been an Active Member of the IEEE Signal Processing Society and the IEEE Engineering in Medicine and Biology Society. He was a recipient of the International Travel Grant (Young Scientist) by the Department of Science and Technology, Government of India. He is serving as a peer reviewer for many reputed international journals and conferences, including IEEE TRANSACTIONS ON INSTRUMENTATION AND MEASUREMENT, IEEE ACCESS, IEEE SENSOR JOURNAL, *Biomedical Signal Processing and Control* (Elsevier), *Computers and Electrical Engineering* (Elsevier), *International Journal of Machine Learning and Cybernetics* (Springer), *International Journal of Electronics Letters* (Taylor and Francis), and *Frontiers in Physiology*.

SHRIVISHAL TRIPATHI (Senior Member, IEEE) received the B.Tech. degree in electronics and communication engineering from the Dr. K. N. Modi Institute of Engineering and Technology, Ghaziabad, India, in 2009, the M.E. degree in electronics and electrical communication from the PEC University of Technology, Chandigarh, India, in 2011, and the Ph.D. degree from the Electrical Engineering Department, IIT Jodhpur, Rajasthan, India, in 2015. He is currently an Assistant Professor with the International Institute of Information Technology, Naya Raipur. His main research interests include RF and microwave, artificial intelligence in electromagnetics, machine/deep learning in circuit design, signal modulation/demodulation techniques, the IoT, and ad-hoc networks. He has completed many projects as PI and Co-PI sanctioned by the different funding agencies. He is the focal person coordinator of IIRS-ISRO of Government of India outreach program. In addition to that contributed to the ''National Rogue Drone Policy'' of Government of India.

AVINASH VUJJI received the B.Tech. degree in electrical and electronics engineering from Jawaharlal Nehru Technological University, Hyderabad, India, in 2008, the M.Tech. degree in power and industrial drives from Jawaharlal Nehru Technological University, Kakinada, India, in 2013, and the Ph.D. degree from the Department of Electrical Engineering, National Institute of Technology (NIT), Kurukshetra, India, in 2023. His research interests include power electronics, control of electrical drives, machine learning, the IoT, and deep learning. He is currently an Associate Professor with the Vignan's Institute of Engineering for Women. He has published several articles in journals and conference proceedings of international repute. He is serving as a peer reviewer for many reputed international journals and conferences, including *International Journal of Circuit Theory and Applications*, *Electric Power Components and Systems*, and *Distributed Generation & Alternative Energy Journal*.

RAM BILAS PACHORI (Senior Member, IEEE) received the B.E. degree (Hons.) in electronics and communication engineering from Rajiv Gandhi Technological University, Bhopal, India, in 2001, and the M.Tech. and Ph.D. degrees in electrical engineering from IIT Kanpur, India, in 2003 and 2008, respectively. Before joining IIT Indore, India, he was a Post-Doctoral Fellow with the Charles Delaunay Institute, University of Technology of Troyes, France (2007–2008) and an Assistant Professor with the Communication Research Center, International Institute of Information Technology, Hyderabad, India (2008–2009). He was an Assistant Professor (2009–2013) and an Associate Professor (2013–2017) with the Department of Electrical Engineering, IIT Indore, where he has been a Professor, since 2017. He is also associated with the Center for Advanced Electronics, IIT Indore. He was a Visiting Professor with the Department of Computer Engineering, Modeling, Electronics and Systems Engineering, University of Calabria, Rende, Italy, in July 2023; Faculty of Information & Communication Technology, University of Malta, Malta, from June 2023 to July 2023; Neural Dynamics of Visual Cognition Laboratory, Free University of Berlin, Germany, from July 2022 to September 2022; and School of Medicine, Faculty of Health and Medical Sciences, Taylor's University, Malaysia, from 2018 to 2019. Previously, he was a Visiting Scholar with the Intelligent Systems Research Center, Ulster University, Londonderry, U.K., in December 2014. His research interests include signal and image processing, biomedical signal processing, non-stationary signal processing, speech signal processing, brain-computer interface, machine learning, and artificial intelligence and the internet of things in healthcare. He was an Associate Editor of IEEE TRANSACTIONS ON NEURAL SYSTEMS AND REHABILITATION ENGINEERING (2021-2024). Currently, he is an Associate Editor of ELECTRONICS LETTERS, IEEE OPEN JOURNAL OF ENGINEERING IN MEDICINE AND BIOLOGY, Computers and Electrical Engineering, and Biomedical Signal Processing and Control, and an Editor of IETE *Technical Review journal*. He is a Fellow of IETE, IEI, and IET. He has authored the textbook titled ''Time-Frequency Analysis Techniques and their Applications'' (CRC Press, 2023). He has 339 publications, which include journal articles (213), conference papers (89), books (10), and book chapters (27). He has also eight patents, including one Australian patent (granted) and seven Indian patents (published). His publications have been cited approximately 17000 times with h-index of 70 according to Google Scholar.